UNIVERSIDADE DE LISBOA
FACULDADE DE CIÊNCIAS
DEPARTAMENTO DE FÍSICA

Improving medical imaging handling for radiotherapy using Velocity

Mafalda Mantero Morais Duarte Silva

Mestrado Integrado em Engenharia Biomédica e Biofísica
Perfil em radiações em diagnóstico e terapia

Dissertação orientada por:
Prof. Dr. Luis Peralta e Dra. Sandra Vieira

2018

"*Not all of us can do great things. But we can do small things with great love."*
Mother Theresa of Calcutta

ACKNOWLEDGMENTS

This dissertation would not have been concluded without the support of several people whom I would like to thank.

First, I would like to thank to all the Radiation Therapy Department team at Champalimaud Foundation who received and accompanied me during my internship. Specially to Dr. Sandra Vieira who guided and supervised my dissertation always with a smile on her face and to Dr. Joep Stroom and Dr. Marco Possanzini who were always available to help.

Thank you, Sara Guerreiro, for being my daily company and for all the advice and availability showed throughout this internship.

I am also thankful for Professor Luis Peralta orientation, patience and dedication.

Thank you Prof. Marília Antunes, Prof. Patricia Bermudez and Ricardo Sousa for the accessibility and help.

Thank you, Dr. Esmeralda Poli and Prof. Hugo Ferreira, for the helpful and constructive comments about my dissertation.

A huge thank you to my parents and brothers, who helped me since childhood and taught me how to organize and structure work and educated me with the values of hard work, effort, honesty and altruism.

I would like to thank to my best college friends, Amanda Silva and Nuno Silva, without whom it would not have been possible to conclude this journey.

Thank you, Carolina Fraga and Mafalda Freitas, for the hours spent reading my dissertation and for all the tips and advices.

Thank you to all my friends, specially to Francisco Marques, who heard me talking about radiation and cancer even when they did not want to, and who were always there for me.

ABSTRACT

The first step in Intensity Modulated Radiation Therapy (IMRT) treatments is to acquire a Computed Tomography (CT) to plan Radiation Therapy – the planning CT (pCT). Thereafter, before an image guided session of EBRT, a Cone Beam CBCT is acquired making sure the patient is correctly positioned as was while acquiring the pCT. However, there are frequent changes in shape and size of different organs during treatment, meaning that the planned dose might not be the delivered. If these changes are significant, a treatment re-plan may be required, which is time consuming.

This situation can be avoided, since re-planning is sometimes taken as precaution due to specialist uncertainty about the exact distribution of the delivered dose.

Deformable image registration (DIR) is a possible solution to know the dose distribution throughout the entire treatment. The latter can be performed by deforming the planning CT on each daily CBCT and posteriorly calculate the actual delivered dose using the reshaped CT's. It is not advisable to use the CBCT's due to the low quality of image.

In this project, the benefits of using DIR on clinic are going to be explored, by firstly evaluating DIR quality on pelvic CT-CBCT scans.

The study cases enrolled in this dissertation were diagnosed with cervical or endometrial cancer. These patients accepted being part of a clinical study implemented at and approved by the ethical commission of Champalimaud Foundation, which suggests the implementation of Stereotactic Body Radiation Therapy (SBRT) instead of Brachytherapy, to avoid tumour recurrence. Using DIR, it is also going to be analysed the deformation magnitude and consistency of these patients during treatment as well as calculated the actual delivered dose to the PTV and CTV.

For DIR purposes, it is going to be use Velocity® in this project, a software developed by Varian Medical Systems. The study cases planning CT's are going to be deformed to the CBCT form using two DIR methods: one intensity-based and one intensity-based and feature based. For dose calculation purposes, Eclipse (Varian Medical Systems) is going to be used.

Key-words: Radiation Therapy; Cone Beam Computed Tomography; Computed Tomography; Deformable Image Registration; Gynaecological cancer.

RESUMO

Este projeto foi desenvolvido na Fundação Champalimaud, Lisboa, Portugal, na área de radioterapia.

A radioterapia é utilizada para tratar neoplasias bem localizadas, e pode ser usada como complemento de cirurgia e/ou quimioterapia. Envolve a utilização de radiação ionizante para afetar o tumor, e destruir as células cancerígenas. Há dois principais tipos radioterapia: radioterapia externa (EBRT) e braquiterapia. Neste projeto, vão ser exploradas radioterapia externa e braquiterapia, uma vez que estas são as técnicas utilizadas em doentes com cancro ginecológico, doentes incluídas num estudo clinico aprovado pela comissão ética da fundação Champalimaud, e os nossos casos de estudo.

O primeiro passo em tratamentos de radioterapia externa (EBRT) passa por adquirir uma imagem de tomografia computorizada convencional (CT) para planear o tratamento de radioterapia – o CT de planeamento (pCT). Na Fundação Champalimaud, são realizados dois tipos de EBRT: Arcoterapia Volumétrica Modulada (VMAT) e Radioterapia Modulada por Intensidade de ângulos fixos (IMRT). Para propósitos de localização tumoral, estes tipos de radioterapia são complementados por radioterapia guiada por imagem (IGRT).

Nesta instituição, o CT de planeamento adquirido é um CT espiral, com qualidade alargada, que permite visualizar com clareza a área que irá ser irradiada. Após diagnosticar o tumor, o radio-oncologista utiliza o *software* Eclipse® (*Varian Medical Systems*) para contornar as estruturas relevantes para planear o tratamento e para prescrever uma determinada dose para irradiar o tumor, com auxílio de outras imagens médicas como ressonância magnética. No caso de tratamentos de EBRT, é crucial prescrever uma dose ao PTV (volume de planeamento de alvo), uma vez que este é uma extensão do CTV (local de suspeita infiltração do tumor) e que tem em conta potenciais variações geométricas durante o tratamento.

Com o Eclipse®, utilizando o pCT, é possível fazer o planeamento de tratamento. Depois de fazer o controlo de qualidade do tratamento (utilizando o *ArcCheck* e/ou *EPID*) o doente está pronto para ser tratado.

Antes de cada sessão de radioterapia externa guiada por imagem (IGRT), é adquirida uma imagem de CT de feixe cónico (CBCT) para garantir que o doente está corretamente posicionado, como enquanto se adquiriu o pCT. O CBCT é uma imagem que tem menos qualidade que o CT espiral e que permite administrar menos dose de radiação ao doente, permitindo ainda assim garantir que o doente está na posição correta para ser tratado.

No entanto, há mudanças frequentes na forma e tamanho dos diferentes órgãos durante o tratamento. Desta forma, a dose planeada pode por vezes não ser a que é realmente administrada. Quando as mudanças são significativas, é por vezes necessário recorrer ao replaneamento de tratamento, o que pode resultar num prolongamento do processo clínico e ocupação dos recursos humanos.

O replaneamento pode ser evitado, uma vez que é por vezes realizado por precaução devido à incerteza dos especialistas, da distribuição exata de dose administrada ao doente.

No registo deformável de imagens (DIR), pretende-se transformar uma imagem ("imagem em movimento") numa outra ("imagem fixa"). Há três tipos de DIR, que utilizam diferentes funções objetivas para encontrar a melhor correspondência entre a imagem em movimento e a fixa: DIR baseada na intensidade dos pixéis de ambas as imagens (pressupõe que as duas apresentam intensidades semelhantes em iguais pontos); DIR baseada em algumas características (recorre a determinadas características das imagens, como estruturas semelhantes contornadas em ambas); DIR híbrida (resulta na conjugação dos dois métodos anteriores).

O DIR é uma potencial ferramenta para saber a exata distribuição de dose de um doente durante o tratamento. É possível deformar o pCT à imagem de cada CBCT adquirido, e depois calcular-se a dose

administrada nos CT's deformados. Isto devido ao facto de não ser possível calcular dose nos CBCT's devido à falta de qualidade de imagem, o que pode resultar em erros associados.

Neste projeto, os casos de estudo são doentes diagnosticadas com cancro ginecológico: do colo do útero ou do endométrio. O diagnóstico destas doentes é feito em primeiro lugar através de uma consulta, da realização de um ultrassom trans-vaginal, biópsia do tumor, CT abdominal-pélvico e ressonância magnética pélvica. Quando o diagnóstico é estabelecido, o estádio do tumor é avaliado de acordo com: diferenciação das células dos tecidos, alastramento e metastização, idade da doente, e invasão do espaço linfo-vascular (LVSI). A aquisição de CT's torácicos ou abdominais superiores é indicada para detetar eventuais metástases distantes. Pode ser adquirida uma imagem de Tomografia por Emissão de Positrões (PET) quando se está na presença de um cancro ativo, para estadear metástases distantes e para confirmar a extensão da doença.

Após o primeiro tratamento de EBRT ou quimioterapia adjuvante, a braquiterapia é o tratamento *stantard* a ser administrado a doentes com cancro do colo do útero ou endométrio, para evitar a recorrência tumoral. No entanto, as doentes incluídas nesta dissertação aceitaram fazer parte de um estudo clínico implementado e aceite pela comissão de ética da Fundação Champalimaud: utilizar um *boost* de radioterapia estereostática (SBRT) VMAT no lugar de braquiterapia em doentes ginecológicos. A SBRT implica a prescrição de uma alta dose de radiação para os tumores, e requer imobilização ou monitorização da doente, uma vez que pequenos movimentos podem danificar a precisão de dose administrada. De acordo com o estádio da doença, e dependendo se o útero é passível de ser removido por cirurgia, as doentes de cancro do colo do útero ou endométrio podem passar por três ou cinco frações de SBRT. Às doentes de três frações, foi possível remover o útero através de cirurgia, enquanto que as doentes de cinco frações ainda apresentam útero.

Neste projeto, foi utilizado para DIR, o Velocity® (*Varian Medical Systems*). Para cálculos de dose, foi utilizado o Eclipse®.

Foram primeiro estudados os benefícios de usar DIR na clínica, avaliando em primeiro lugar a qualidade da DIR.

Após a validação do *software* para os casos de estudo, para transformar os pCT's à imagem de cada um dos CBCT's, recorreu-se a dois métodos de DIR. Os dois rCT's resultantes, correspondentes ao mesmo CBCT foram depois comparados, para que fosse possível decidir qual dos métodos era o mais indicado para os casos de estudo. Os dois métodos utilizados do Velocity® foram: *CBCT Corrected Deformable* (indicado para registo de imagem pCT-CBCT; função objetiva baseada na intensidade dos pixéis) e *Structure Guided Derformable* (função objetiva híbrida).

Para as imagens abdomino-pélvicas de doentes com cancro ginecológico, o método que melhor resultou, foi o *Structure Guided Deformable*. No entanto, por vezes o *CBCT Corrected Deformable* teve melhores resultados, o que levou a concluir que quando os resultados não são bons o suficiente quando utilizando o primeiro, se deve utilizar o segundo.

Quando os pCT deformados eram considerados aprovados, ou seja, estavam em conformidade com o CBCT correspondente, era possível utilizar os mesmos para realizar cálculos de dose. A avaliação foi realizada considerando apenas a região do PTV, uma vez que esta é a zona com relevância clínica. Os pCT's deformados no Velocity® foram exportados para o Eclipse® para proceder ao cálculo da dose em cada pCT deformado. O plano original de tratamento foi copiado para os mesmos, para replicar a situação de tratamento. O cálculo da dose dos rCT's sobreposta no pCT permitiu a avaliação da conformidade das doentes ao longo do tratamento, e também a preparação do passo seguinte.

As doses calculadas no Eclipse® nos rCT's deformados foram importadas para o Velocity®, onde se procedeu à deformação da dose dos rCT's para o pCT (através da matriz de deformação anteriormente criada) e depois se procedeu à soma das doses deformadas, permitindo aceder à dose realmente administrada em todos os tratamentos.

Recorrendo à DIR, avaliou-se também a dose realmente administrada ao PTV e CTV das doentes incluídas no estudo clínico, e foi estudado se a dose administrada às estruturas de risco se encontrava dentro dos limites clinicamente aceites.

Em relação à conformidade das doentes durante todo o tratamento, parece existir uma relação entre a mesma e a curva de aprendizagem do protocolo implementado no estudo clínico. No entanto, também aparenta ser possível que a conformidade das doentes esteja relacionada com o número de frações SBRT. O mesmo se verificou com a dose realmente administrada. A maior percentagem de dose administrada em relação à planeada, no CTV e PTV, evidencia estar correlacionada tanto com o tipo de doente, como com a curva de aprendizagem. Também foi analisada a dose administrada às seguintes estruturas de risco: intestino delgado, parede do reto e parede da bexiga. A dose administrada a estas estruturas, encontrou-se dentro dos limites aceites clinicamente.

O Velocity® provou ser um *software* de fácil utilização, e que é útil para a realização de DIR em registo pCT-CBCT de imagens de doentes com cancro ginecológico.

Para futuro trabalho, é importante estudar DIR noutros tipos de imagens, e reunir mais doentes tratadas com SBRT para evitar recorrência tumoral (endométrio ou colo do útero), para conclusões mais precisas acerca deste método. O Velocity® também pode ser potencialmente utilizado para implementar radioterapia adaptativa na clínica.

Palavras-chave: Radioterapia; Tomografia Computorizada; Tomografia Computorizada de Feixe Cónico; Registo Deformável de Imagens; Cancro ginecológico.

CONTENTS

LIST OF FIGURES

LIST OF ABBREVIATIONS

ADD	**A**ctual **D**elivered **D**ose
CBCT	**C**one **B**eam **C**omputed **T**omography
CC	**C**orrelation **C**oefficient
CD	CBCT **C**orrected **D**eformable
CF	**C**hampalimaud **F**oundation
CT	**C**omputed **T**omography
CTV	**C**linical **T**arget **V**olume
DIR	**D**eformable **I**mage **R**egistration
DMP	**D**eformable **M**ulti-**p**ass
DVF	**D**eformation **V**ector **F**ield
DVH	**D**ose **V**olume **H**istogram
$\mathbf{E_k}$	**K**inetic **E**nergy
EBRT	**E**xternal **B**eam **R**adiation **T**herapy
EPID	**E**lectronic **P**ortal **I**maging **D**evice
GTV	**G**ross **T**umour **V**olume
HU	**H**ounsfield **U**nits
IGRT	**I**mage **G**uided **R**adiation **T**herapy
IMRT	**I**ntensity **M**odulated **R**adiation **T**herapy
IR	**I**mage **R**egistration
LINAC	**L**inear **P**article **A**ccelerator
LVSI	**L**ymphovascular **S**pace **I**nvasion
$\mathbf{m_{conformality}}$	**M**ean **c**onformality
MI	**M**utual **I**nformation
MLC	**M**ultileaf **C**ollimators
MR	**M**agnetic **R**esonance
N	Sample size
OAR	**O**rgans **a**t **R**isk
pCT	**P**lanning **CT**
PET	**P**ositron **E**mission **T**omography
POI	**P**oint **o**f **I**nterest
PRV	**P**lanning organ-at-**r**isk **V**olume
PTV	**P**lanning **T**arget **V**olume
rCT	**R**eshaped **CT**
RIR	**R**igid **I**mage **R**egistration
ROI	**R**egion **o**f **I**nterest
RT	**R**adiation **T**herapy
SBRT	**S**tereotactic **B**ody **R**adiation **T**herapy
SD	**S**um **D**ose
SGD	**S**tructure **G**uided **D**eformable
SSD	**S**um of **S**quared **D**ifference
VMAT	**V**olumetric **M**odulated **A**rc **R**adiation **T**herapy
W	Observed statistic
XR	**X**-**R**ay
α	Significance level

LIST OF TABLES

1. INTRODUCTION

In this project the advantages of using Velocity® on clinic at Champalimaud Foundation (CF) are assessed. The use of this software and Deformable Image Registration (DIR) may improve clinical workflow, avoiding re-planning External Beam Radiation Therapy treatments unnecessarily.

This study will focus on treatments for patients with gynaecological cancer (cervical or endometrial) using DIR image processing. These patients have been treated with an innovative boost treatment of Stereotactic Body Radiation Therapy (SBRT) instead of Brachytherapy, as suggested by a clinical study in course, approved by CF ethical commission.

1.1. CANCER

Tumours are caused by human cells mutations, leading to changes in regulation mechanisms of cell proliferation (increased stimulation of cell division) and/or apoptosis (decreased stimuli that interrupt cell division). In the cell division process, if some mutation occurs at the alleles of tumour suppressor genes, in proto-oncogenes, or in other responsible for cell proliferation, it will possibly lead to the formation of a tumour [1].

The proto-oncogene mutation will continuously stimulate cell division. Also, a mutation of a tumour suppressor gene can cease it inhibitory action in the proliferative stimulation of proto-oncogenes, contributing to the development of a neoplasm.

If benign, tumours are usually well localized, have a regular shape, do not metastasize and respond well to treatment. These do not invade adjacent tissues, even though can compress the surrounding structures, contrary to malignant tumours, which invade adjacent tissues, have a faster cell proliferation, where metastasizing usually occurs and have an irregular shape. Sometimes, malignant tumours may reoccur after treatment [2].

When lumps are found in medical images such as Computed Tomography (CT), X-ray (XR) or Magnetic Resonance (MR), usually, a biopsy is done by removing a piece of the protuberance so that it is possible to analyse the tumour and confirm the diagnosis. The analysis and tests of these samples can confirm the cancer diagnosis and help in the choice of treatment method [3].

1.2. CANCER THERAPIES – GYNAECOLOGICAL CANCER

When a cancer is diagnosed, a treatment plan will be outlined depending on the type and stage of development of the patient's tumour. There are many options of treatment for malignant tumours, but usually, gynaecological cancer patients are treated with surgery, chemotherapy and/or radiation therapy [4].

Surgery

When a localized primary tumour is diagnosed, the first and most efficient treatment is surgery. Since this therapy operates by zero-order kinetics, and kills all the extracted cells, it is the therapy which cures more patients with tumours with the stated conditions. Usually, surgery is performed with other complementary therapies such as chemotherapy or radiotherapy [5].

Chemotherapy

This treatment involves the use of chemical cytostatic drugs (anticancer drugs) which destroy cancer cells, by stopping them from multiplying or growing. These drugs are taken by infusion into a vein or as tablets. The anticancer drugs travel through the bloodstream, acting in all parts of the body. This therapy can be used to eliminate all the cancer, as a complement of surgery or radiation therapy, or even to shrink tumour before surgery. Sometimes, can be performed to relieve symptoms or to slow down the tumour if there's no cure [6], [7].

Radiation Therapy

This technique is used to treat well localized neoplasms and can be used as complement of surgery and/or chemotherapy. It involves the use of ionizing radiation to affect the tumour, and destroy cancer cells [8].

Each patient must have a treatment plan made by a group of professionals which includes radiation oncologists and physicists. This team prescribes a plan of dose, that must be delivered to a specific patient, with a specific tumour [8].

There are three types of radiation therapy (RT): radioisotope therapy (systemic injection that has been designed to target disease), brachytherapy (insertion of radiation-emitting sources near the tumour) or external beam radiation therapy – EBRT – (external application of radiation beams to treat the cancer) [8]. In this chapter, EBRT and brachytherapy will be explained, since these are the radiation therapy treatments used to treat endometrial and cervical cancer.

1.3. RADIATION THERAPY MODALITIES

1.3.1. EXTERNAL BEAM RADIATION THERAPY

In External Beam Radiation Therapy (EBRT) high energy beams from outside the body into the tumour are used, usually irradiated by linear particle accelerators (LINACs).

X-rays, produced by electrons, are used in EBRT and can be superficial ($10 \leq E_k \leq 100$ keV), orthovoltage ($100 \leq E_k \leq 500$ keV) or megavoltage ($E_k \geq 1$ MeV). Superficial or orthovoltage, are produced with X-ray tubes while megavoltage are produced commonly with LINACs (Figure 1.1) [9].

Linear Particle Accelerator (LINAC)

LINAC's respect the two basic accelerators conditions: the particle to be accelerated is charged and an electric field is provided in the direction of the particle acceleration. The type of accelerator depends on the way it produces the accelerating electric field and how the field acts on the particles to be accelerated. Considering the accelerating electric field, there are two main classes of accelerators: electrostatic and cyclic [9].

Medical LINACs (Figure 1.1) are cyclic accelerators: the electric fields are variable and non-conservative and associated to a variable magnetic field. These can produce beams by using high-frequency electromagnetic waves (Microwaves: $10^3 - 10^4$ MHz; Vast majority S frequency band) to accelerate electrons to kinetic energies from 4 to 25 MeV. The beam can penetrate the human body to treat either superficial or deep-seated tumours [9], [10].

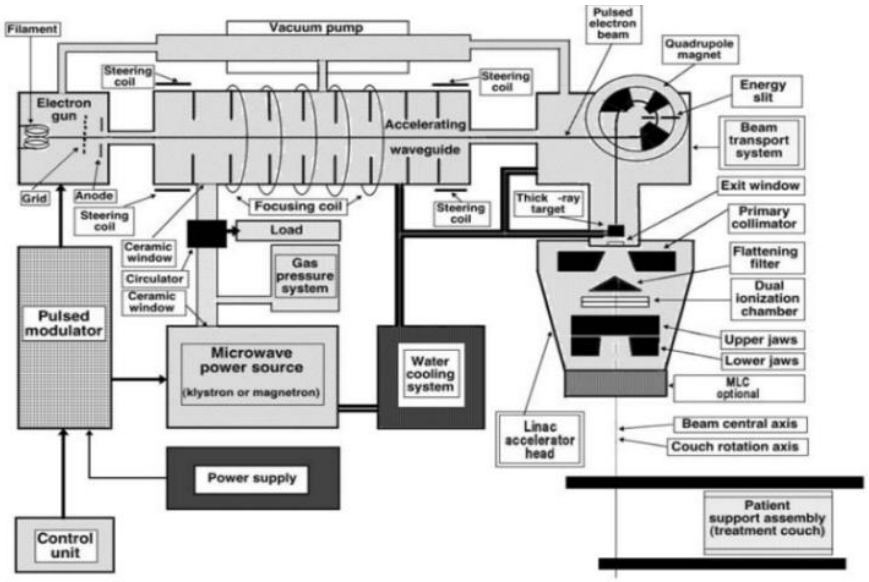

Figure 1.1: Typical medical LINAC (Adapted from [9])

The accelerating waveguides are evacuated structures where the electrons are accelerated and follow straight trajectories. The magnetrons and klystrons produce the microwaves, generating the high-power radio frequency fields used for acceleration in the accelerating waveguides. The deceleration of the electrons, when they hit the target leads to the emission of bremsstrahlung radiation (X-rays photons) [9].

The last generation LINAC's provide high energy photons (XR) and electrons. The introduction of multileaf collimators (MLC) in this generation allowed photon beam intensity modulation and full dynamic conformal dose delivery with intensity modulated beams.

The types of external beam radiation therapy performed at Champalimaud Foundation are Intensity Modulated Radiation Therapy (IMRT) and Volumetric Modulated Arc Radiotherapy (VMAT). These are complemented with Image Guided Radiation Therapy, since CBCT scans (Chapter 1.5.4.1) are acquired before any treatment fraction, allowing the patient position adjustment according to the planning positioning. By using the Multileaf Collimators, on IMRT or VMAT it is possible to change the beam strength in certain areas, making it possible to deliver a stronger dose in the tumour. On IMRT the gantry stops at certain positions, MLCollimators are reshaped according to tumour's shape in that location and then the cancer is irradiated. On VMAT, the gantry moves continuously while irradiating, and the MLCollimators are continuously reshaped in conformity with tumours 3-dimensional shape [11].

The referred EBRT methods performed in CF use only X-rays (photons) to treat neoplasms. To treat superficial tumours, a phantom layer of "skin", names *bolus*, is used in order to guarantee the interaction of the X-rays with the superficial tumour.

X-ray radiation is ionizing, and interacts indirectly with matter, contrary to electrons, protons, alpha particles or heavy ions. The radiation interacts with other molecules, and by originating free radicals, causes breakage of chemical bonds or oxidation of the molecules, leading to DNA breakage. This DNA breakage, and the changes in the cell molecules, induce cellular death [12]. There is also the direct breakage of DNA strands by radiation, which also induces cellular death.

1.3.2. BRACHYTHERAPY

Brachytherapy is a RT method performed at short distance with small, encapsulated radionuclide sources. It is commonly used as a boost treatment in cervical/endometrial cancer cases. These sources are placed directly into/near the region to be treated, and emit, most commonly, photons to destroy the tumour[a]. In case of gynaecological cancers, a device named tandem is insert into the vagina and the source emits the photons, as seen in Figure 1.2 [13]**.** The dose can be delivered continuously, over a brief period or over the lifetime of the source to a complete decay. Photons interaction with tumours was described in the previous section [9].

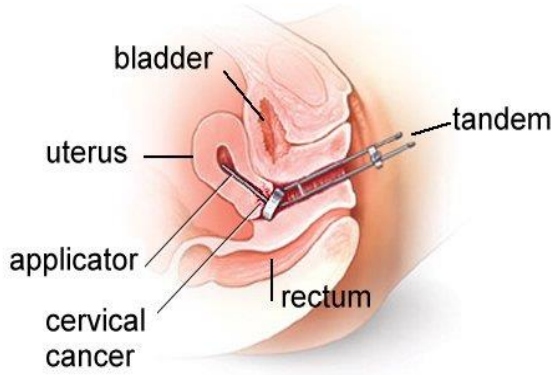

Figure 1.2: Uterus Intracavitary Brachytherapy (Adapted from [13]).

There are two types of brachytherapy: intracavitary and interstitial, both implemented in cases of cervical and endometrial cancers. In intracavitary brachytherapy, the sources are positioned near the tumour volume and the treatment is always temporary, of short duration. The fractions are delivered typically 1-2 times per week [14]. However, in interstitial brachytherapy, the sources are implanted in the tumour volume and the treatments may be temporary or permanent and usually the treatment is performed in a single session [9], [14].

In Portugal, to treat cervical and endometrial cancer, patients can pass through surgery (hysterectomy), chemotherapy and/or EBRT. Brachytherapy is still the first choice when, after the first phase of treatment, is needed to boost the tumour with RT to avoid tumour recurrence [15].

Even though this treatment enables higher localized dose delivery when compared with EBRT, it can only be used when the tumour is small and well localized [9].

1.4. INDIVIDUAL PLANNING

RT treatment planning to a specific tumour must not be performed without considering several vital facts. When the patient is diagnosed with cancer, a reference CT is used to plan the treatment: the planning CT (pCT). The process of planning includes contouring the organs at risk plus tumour, beam set-up on the pCT and verification of the plan (which includes the total dose delivered to the patient). The latter is performed by the physicist. The final plan approval is given by the radiation oncologist. At CF, the delimitation of structures is performed using Eclipse®, v. 13.6 1996-2015 Varian Medical Systems, Inc.

[a] β or neutron emitting sources are used in specific situations.

Quality assurance is performed before the treatment delivery (at CF with ArcCheck, Sunnuclear Corporation, and/or EPID, Varian Medical Systems). Before any session of treatment, the patient is submitted to a CBCT scan (Chapter 1.5.4.1), to make sure of the correct set-up position.

In RT planning phase the following ROI's are considered: gross tumour volume (GTV – volume of known tumour infiltration), clinical target volume (CTV – suspected tumour infiltration), organs at risk (OAR – healthy organs that can be affected by the treatment), planning organ-at-risk volume (PRV) and planning target volume (PTV). PRV and PTV are created to ensure that the prescription restrictions match the absorbed dose delivered to the OAR and CTV, respectively. It is important to define PTV, PRV and GTV independently of irradiation techniques, since for delineation of volumes the type of radiation employed is irrelevant. The following parameters combined are important to decide the treatment plan quality: total amount of dose delivered to a specific tumour and surrounding organs, number of sessions and the time between each session, overall time, patient position on each treatment [16]. In case of EBRT treatments, it is crucial to prescribe a specific amount of dose to the PTV, since this structure is a CTV's "extension". The prescription of a certain amount of dose to the PTV, assures the delivery of that amount of dose to the CTV.

At CF, the dose calculations are performed in Eclipse®, which uses the contours and restrictions made by the radiation oncologist, as well as the CT scans Hounsfield Units. After discussing and deciding the final plan, it is possible to analyse the planned dose distribution by displaying the dose in colour scales on the CT plan and by displaying Dose Volume Histograms (DVH), which supply information about the delivered dose at each percentage of volume of the regions of interest.

A plan dose distribution of one of this dissertation study cases is shown in Figure 1.3.

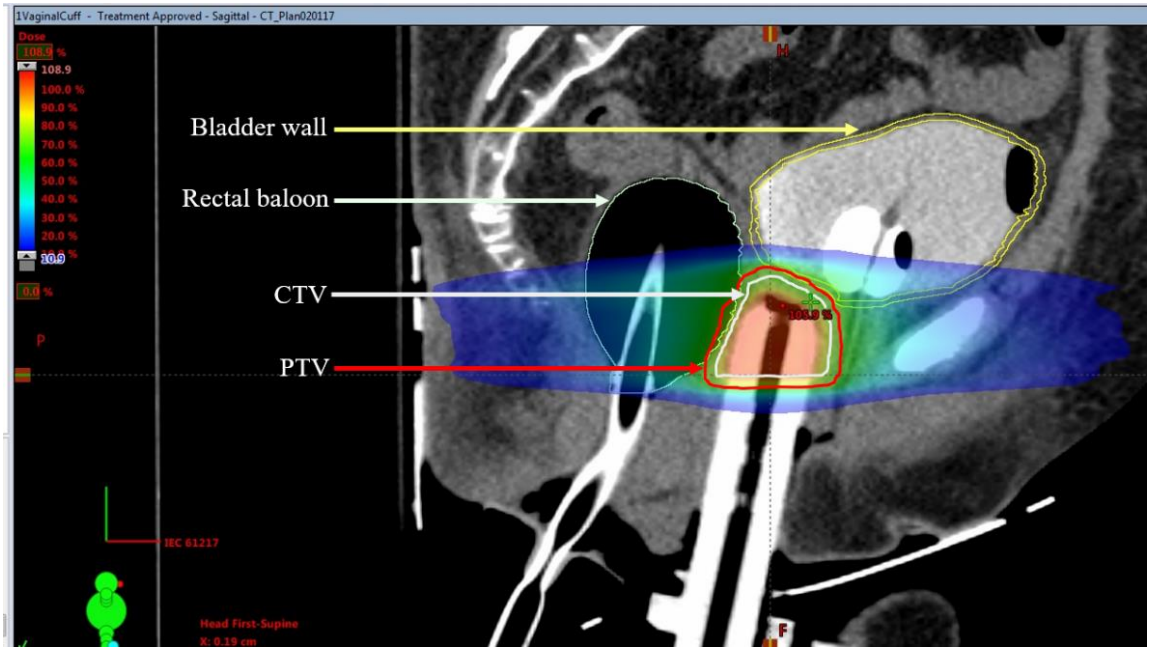

Figure 1.3: Planned dose distribution of a patient treated with SBRT: 3 x 7.5Gy.

1.5. MEDICAL IMAGING - GYNAECOLOGICAL CANCER

1.5.1. MAGNETIC RESONANCE IMAGING (MRI)

Magnetic Resonance images provide a spatial map of the hydrogen nuclei on tissues. The principle behind MRI consists on the orientation of the hydrogen nuclei spin by the action of a magnetic force field, which can organize them as parallels or anti-parallels. An MRI image intensity depends on the physical properties of each tissue and on the number of protons in certain locations [17]. It's an advantageous technique since there is no need of using ionizing radiation – no harm of penetration - and the contrast is high, the images can be acquired in any 2 to 3-dimension plan and the spatial resolution can be 1 mm or less. However, it's an expensive technique, slower than CT and cannot be performed on patients with metallic prostheses or pacemakers [17].

Despite the high quality of image, and the fact that MRI scans are used in the planning phase of EBRT treatment for contouring purposes, CT is still the standard image used when planning EBRT treatments even though MRI has a lot of potential in this field [18], [19].

1.5.2. POSITRON EMISSION TOMOGRAPHY

Positron Emission Tomography (PET) is a method of nuclear imaging technique which allows the functional analysis of the human body, unlike Computed Tomography for example, by creating images portraying the distribution of positron-emitting nuclides in patients. Using PET, it is possible to evaluate not only the location of a disease, but also the metabolism and evolution of it.

This method uses positron-emitting radiotracers (carrier molecules bonded to a radioactive atom), which are different depending on the purpose of the scan, and are injected or inhaled by the patient. [20]–[22]. For instance, the radiopharmaceutical fluorine 18 fluorodeoxyglucose (FDG) injected in patients is used to localize tumours, and metastasis, since these are areas where the consume of glucose is higher [23].

Depending on its carrier molecules, the radiotracers distributes within different tissues. When the radionuclide decays, a positron is emitted, and it scatters through the human body losing energy annihilating with an electron, producing two photons (511 keV) emitted in opposite directions. These photons are detected in coincidence by scintillation detectors arranged in a ring. Images are obtained by back-projection methods, showing the patient's radioactivity map [23], [24].

1.5.3. ULTRASOUNDS

An ultrasound image uses high-frequency sound waves to visualise body structures. The transducer is placed inside the body or directly on the skin and it produces the ultra sounds. The ultra-sounds are reflected when hit some of the body structures and then are detected again by the transducer. Subsequently, the images are formed, based on the amplitude of the detected waves [25]. In case of a transvaginal ultrasound, the probe is inserted into the vagina, to examine ovaries, pelvis or part of the womb, being part of gynaecological cancer diagnosis.

1.5.4. COMPUTED TOMOGRAPHY (CT)

CT scans provide medical imagens with great resolution, of a single plan, without overlap of other plans. As well as radiographies, CT scans use X-rays to obtain the images. However, when obtaining CT scans, there is a synchronized rotation of the X-ray tube and a series of detectors that record one-dimensional projections. The patient is positioned into the gantry, where the radiation is both produced and detected. After radiation detection, the image is obtained by a back projection filtered process [17].

A CT image displays a map of the tissue CT numbers, expressed in Hounsfield Units (HU). The HU [Equation (1.1)] depend on structures linear attenuation coefficient (μ). The analysis of the HU of a pCT is necessary to perform the treatment planning on RT [17].

$$\mathrm{HU} = \frac{\mu_{\mathrm{tissue}} - \mu_{\mathrm{Water}}}{\mu_{\mathrm{Water}} - \mu_{\mathrm{Air}}} \times 1000 \tag{1.1}$$

The difference between spiral and conventional CT (Figure 1.4) is that on spiral CT, the tube can move continuously, making possible to move the table continuously while acquiring data. On conventional CT, a slice is acquired while the tube moves in one direction, and the next slice is obtained while the tube moves in the opposite direction [17].At CF it is used spiral CT.

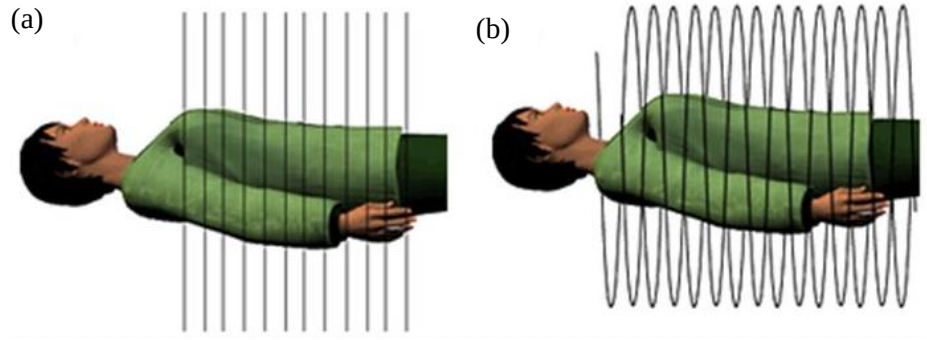

Figure 1.4: Conventional CT (a) vs Spiral CT (a) (Adapted from [26]).

1.5.4.1. Cone Beam Computed Tomography (CBCT)

CBCT scans have less resolution and more image artefacts than CT scans, as it is possible to observe in Figure 1.5.

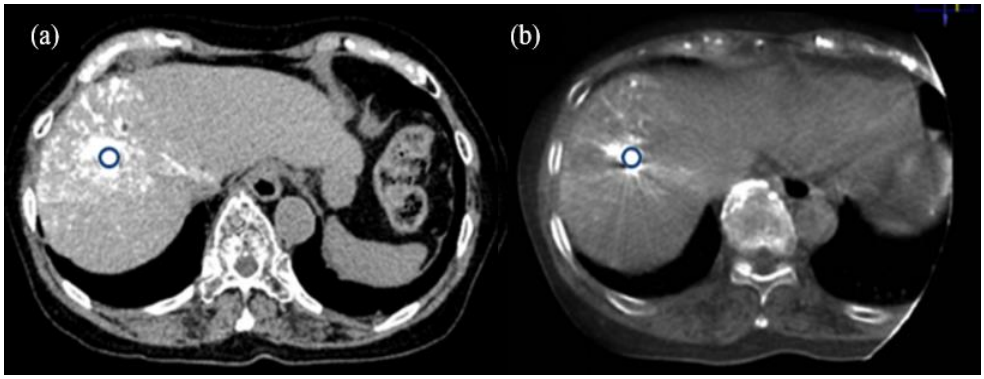

Figure 1.5: Conventional CT (a) vs CBCT (b) image of the liver. (Adapted from [27]).

The main differences between CT and CBCT is that CBCT beam is cone shaped and the detector is an area detector capable of capturing a full volume of image in a single rotation (Figure 1.4 and Figure 1.6) [28].

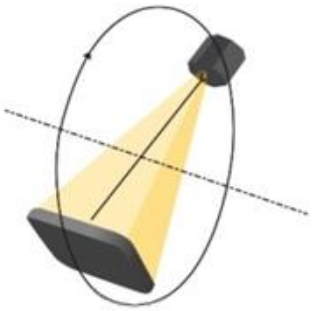

Figure 1.6: Cone Beam CT (Adapted from [29]).

On each RT session, the specialists need to make sure the patient is in the correct position, in order to keep dose delivery as planned, minimising irradiation of healthy structures. In order to guarantee the latter a CBCT exam can be performed before treatment (IGRT) - Figure 1.7.

Even though CBCT is useful before any EBRT fraction treatment to connect patient set-up, it is not enough for planning treatment or for accurate dose calculations. Due to its low resolution, sometimes is not even useful to check tumour evolution [30]. There are studies that suggest dose calculation using CBCT but conclude that it is only possible when using a calibration algorithm, or by combining CBCT with EPID information. Also suggest that these scans can be used to study the impact of anatomy changes, but not for planning treatment [31], [32].

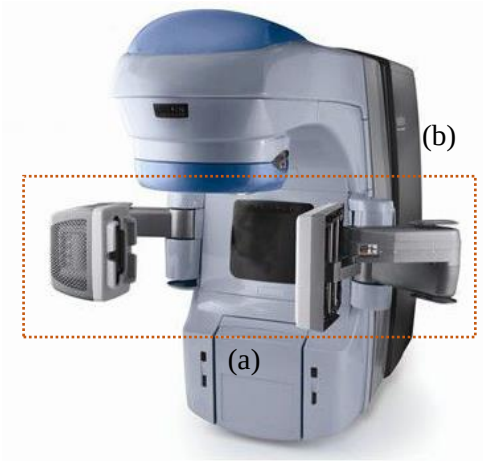

Figure 1.7: LINAC: EPID (a) and CBCT scanner (b). (Adapted from [33]).

On TrueBeam LINAC's (Varian Medical Systems) it is possible to image pelvis using the pelvis spotlight protocol. This protocol uses half rotation of the X-ray source around the patient, differing from the CBCT pelvis protocol which uses a full rotation of the X-ray source. Spotlight protocol results in 1/3 of the weighted CT dose index of a full rotation CBCT, and it is usually used with the aim of reducing the administrated dose to a patient. A spotlight CBCT has a smaller field-of-view in a transversal slice than a full rotation CBCT [34]. The differences between a CBCT and a spotlight CBCT are visible on Figure 1.8.

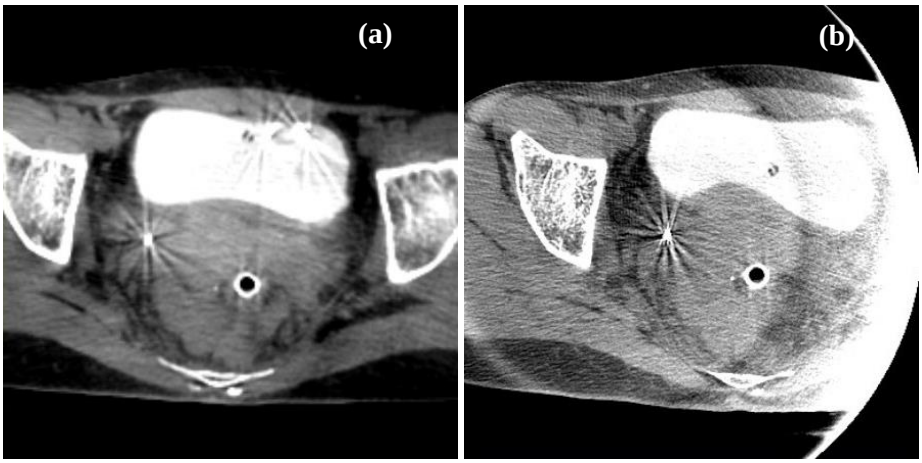

Figure 1.8: CBCT (a) vs spotlight CBCT (b).

1.6. GYNAECOLOGICAL CANCER (ENDOMETRIAL AND CERVICAL)

The uterus anatomy is illustrated in Figure 1.9.

Gynaecological cancer diagnosis is usually performed by gynaecological consultation, trans-vaginal ultrassonography, tumour biopsy, abdominal-pelvic CT scan and pelvic MR. When the diagnosis is established, the stage of the tumour is evaluated according to: differentiation of tumour tissue cells, spreading and metastasis, age of patient and lymphovascular space invasion (LVSI). Thoracic and superior abdominal-pelvic CT scans are indicated to detect eventual distant metastasis. PET can be performed when an active cancer is present to stage distant metastasis and to confirm the extent of locoregional disease. The stages of endometrial and cervical cancer tumours are shown in Table 1.1 and Table 1.2. On Table 1.3 it is possible to find the risk of relapse associated with type in endometrial cancer, cervical cancer risk of relapse is usually not relevant for planning SBRT, that is why it is not explored.

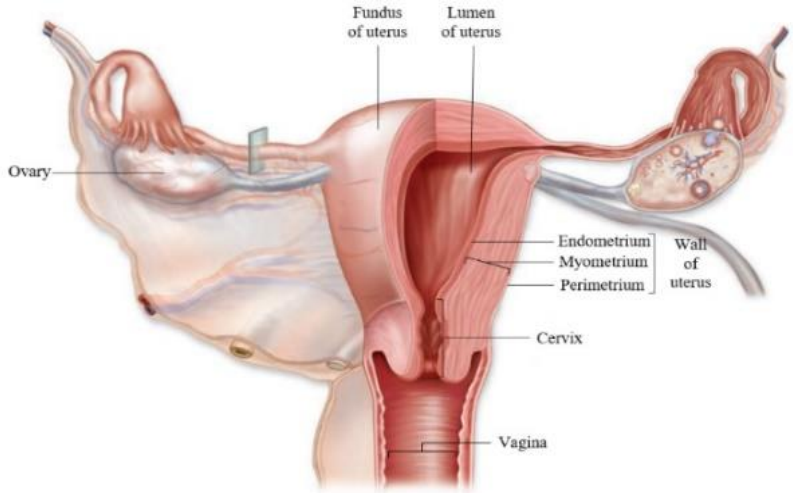

Figure 1.9: Uterus (Adapted from [28]).

If the treatment of a gynaecological patient is RT, clinical examination of the radiation oncologist is crucial to identify some cancer characteristics important in treatment planning.

The first step when treating endometrial or cervical cancer, is to examine if it is possible to remove the tumour with surgery with clear surgical margins (which means it is possible to remove the tumour without having cancer cells in the resection margin). Due to anatomy related motives, endometrial cancer, usually is more suitable for surgery than cervical cancers. After surgery or following the first EBRT treatment (usually with 23 sessions), another treatment can be proposed to the patient, with the aim of increasing the therapeutic dose to the vagina, avoiding excessive irradiation of the surrounding organs at risk. This treatment is usually performed using brachytherapy.

Table 1.1: Classification of **endometrial cancer** according to differentiation and spreading of tumour cells (Adapted from [35]).

Grade G	Differentiation of tumour tissue cells
G_X	Impossible to evaluate
G_1	Well
G_2	Moderately
G_3	Poor

Stage (according to FIGO[b] system)			
Stage I (S_I)	Stage II (S_{II})	Stage III (S_{III})	Stage IV (S_{IV})
Cancer only in the uterus or womb; No metastasis.	Tumour has spread from the uterus to the cervical stroma, but not to other parts of the body	Tumour has spread beyond the uterus, but still in pelvic area	Tumour has metastasized to rectum, bladder and/or distant organ
IA: cancer only in the endometrium or less than 1/2 of myometrium			
IB: tumour spread to more than 1/2 of the myometrium			

Table 1.2: Classification of **cervical cancer** according to differentiation and spreading of tumour cells (Adapted from [36]).

Grade G	Cancer cells
G_1	Most like normal cells
G_2	A bit like normal cells

Stage (according to FIGO system)				
Stage 0	Stage I	Stage II	Stage III	Stage IV (S_{IV})
Carcinoma in situ	Invasive carcinoma, confined to cervix	Tumour extension beyond cervix	**IIIA**: Tumour extension to lower third of vagina but not to pelvic side wall	**IVA:** Tumour invasion (Bladder/Rectum)
			IIIB: Tumour extension to pelvic side wall	**IVB:** Distant metastasis

Table 1.3: Risk of relapse associated with type in **endometrial cancer** (Adapted from [35]).

Risk	Types of tumours	Risk	Types of tumours
Low	S_I , $G_{1,2}$, <50% myometrial invasion , No LVSI	High	S_I, G_3, ≥50% myometrial invasion, regardless LVSI status; $S_{II;}$ S_{III}, no residual disease; Non-endometrioid
Intermediate	S_I , $G_{1,2}$, ≥ 50% myometrial invasion, No LVSI	Advanced	S_{III} residual disease S_{IVA}
High-intermediate	S_I, G_3, <50% myometrial invasion, regardless LVSI status; S_I, $G_{1,2}$, LVSI unequivocally positive, regardless of depth of invasion	Metastatic	S_{IVB}

[b] International Federation of Gynaecology and Obstetrics

2. STATE OF THE ART

Same patient medical scans can differ drastically. Not only due to the nature of the image modality, but also given anatomical changes of the same patient. One of the main objectives of using a software such as Velocity® (Varian Medical Systems) is to uniformize images of CT, CBCT, MRI, etc, by using deformable image registration and deforming different scans. Therefore, allowing for a database of different image sets of the same patient in a consolidated view. In this way, the specialists have an easier and faster process of decision-making during the treatment [37].

2.1. IMAGE REGISTRATION (IR)

Image registration is a process to find spatial correspondence between two or more sets of images. It is beneficial during RT treatments: firstly, in tumour delineation phase, when are used different type of scans to contour the tumour and organs at risk; secondly, it is useful to continuously monitor a patient during treatment, using CT-CBCT registration since both patient and tumour may undergo extreme changes.

Considering two sets of images: a fixed image, $F(x)$, and a moving image, $M(x')$. The goal when using Image Registration is to find the best correspondence between these two sets. It is considered a transformation vector $T(x')$, where x' is the position vector (pixel), and $u(x')$ the displacement vector [38]. Image registration finds the best $T(x')$ to minimize the difference between $F(x)$ and $M(T(x'))$, so that this result can be achieved [38]:

$$F(x) = M\big(T(x')\big) = \ M\big(x' + u(x')\big) \tag{2.1}$$

2.1.1. DEFORMABLE IMAGE REGISTRATION VS RIGID IMAGE REGISTRATION

There are two modalities of image registration: rigid (RIR) and deformable (DIR). Rigid registration has six degrees of freedom when referring to image deformation (3 rotational and 3 translational variables). Deformable registration has a greater number of degrees of freedom, which results in a deformation matrix, or deformation vector field. In RIR all the pixels involved in the transformation move/rotate uniformly resulting in a maintained pixel-to-pixel relation before and after transformation. However, in DIR, these pixel-to-pixel relations change after transformation [38], [39].

When no anatomic changes are expected, RIR is very useful in RT. However, in several cases, there are changes in the patient/tumour throughout the whole treatment, which cannot be handled by RIR. With DIR, it is possible to manage local distortion between two image sets, enabling the management of image sets from different day treatments in a uniform way [38].

2.1.2. DIR PROCESS

The first step of the DIR process is to align the moving image ($M(x')$) with the fixed one ($F(x)$) by RIR or affine translation. Next, by using DIR algorithms, the local area of the moving image is registered to the fixed one. The similarity index between the two images is calculated with the objective function. This starts an iterative process, and the deformation vector field (DVF) is generated, according to a transformation model, to form the moving image, which updates the objective function. The optimization algorithm maximizes the similarity index between the deformed moving image and the

fixed one. Until the similarity index target is achieved, this process continues iteratively. The DIR process is exemplified in Figure 2.1 [38].

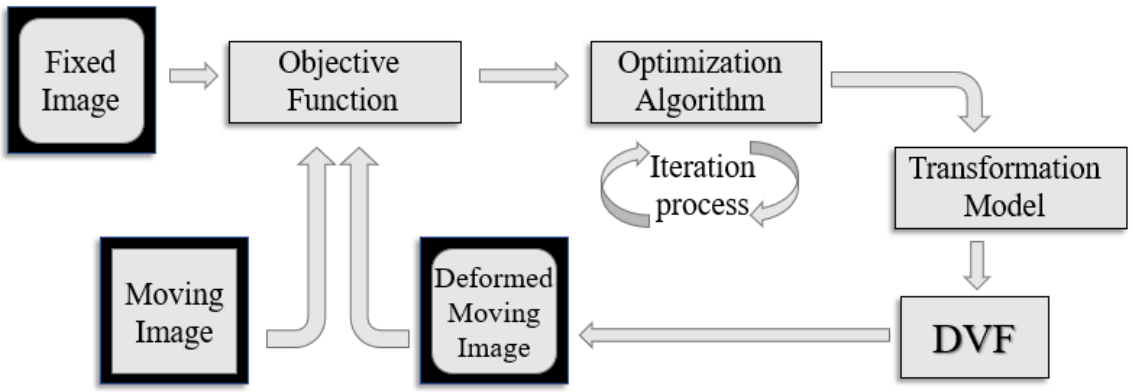

Figure 2.1: Flow chart of DIR process. (Adapted from [38]).

2.1.2.1. Objective Function

As mentioned before, the objective function calculates the similarity index between the fixed and moving image. The type of objective function depends on the way it finds this similarity index. It can be intensity-based, feature-based or hybrid [38].

Intensity-based objective functions calculate the similarity index based on image intensity. These objective functions assume that same structures pixel values among different images are similar. There are some similarity indexes proposed such as Sum of Squared Difference (SSD) of image intensity, Correlation Coefficient (CC) and Mutual Information (MI).

Feature-based objective functions do not depend on image intensity: these are based on considering features in images, such as points of interest (POIs) or contours of ROIs. The simplest way to implement one of these functions is to calculate the squares of the distances between paired POIs in the fixed and moving image.

Hybrid objective functions aim to minimize the limitations of feature-based and intensity-based. Some algorithms were proposed, which combine different terms as similarity and regularization terms. Takayama et al. confirmed the advantages of hybrid-based DIR, by comparing it with intensity-based DIR. They concluded that hybrid based DIR has better results when it comes to comparing CBCT pelvic images [38], [40].

2.1.2.2. Transformation Model

To maximize similarity index, the update of correspondence of POIs/ROIs between two images is based on the transformation model. A deformation model must have a vast number of motion parameters to achieve local transformation [38].

A transformation model can be parametric or non-parametric. On a parametric model, a fine Deformation Vector Field is generated, as a linear combination of its basis functions. On non-parametric models transformation vectors of all points are generated [38]. Since Velocity® only uses a parametric model, this is going to be explored.

The most typical parametric models are spline models. Spline interpolation is a method of constructing, an interpolant based on a discrete set of data points. The spline – interpolant – is a type of

piecewise polynomial. A basis spline (B-spline) has minimal support according to degree, smoothness and domain partition of the spline [38], [41]–[45].

2.1.2.3. DIR APPLICATIONS

Deformable Image Registration has been introduced in the field of radiation therapy and this method has four big applications: 1. Mathematical modelling; 2. Functional imaging; 3. Automatic segmentation and contour propagation; 4. Dose accumulation.

2.1.2.4. Mathematical modelling

Since it is possible to acquire the correspondences between different image sets of the same patients during a full RT treatment using DIR, theoretically it would be possible to create a mathematical model which could predict the evolution of organ deformation, allowing the use of these types of models in RT planning [38].

2.1.2.5. Functional Imaging

Functional imaging is usually acquired with emission tomography methods. However, it is possible to execute a functional image of the lung by using 4D-CT image sets, as suggested in several studies. 4D-CT lung images are used for RT planning, and contain characteristics that can be used to analyse the air in the lungs, due to ventilation[38], [46].

These developed techniques calculated the volume changes (between inhalation and exaltation) of each voxel on the 4D images using the DIR algorithms. With these studies, was possible to find better methods to optimize lung cancer IMRT, by using lung functional images [38], [39].

2.1.2.6. Automatic segmentation and contour propagation

Before RT treatment, the radiation oncologist contours manually all the relevant structures to the treatment plan. This is a process very time-consuming with potential introduced errors which lean on the variability in delineation between different specialists.

Automatic segmentation is an applicability of DIR which enables the reduction of contouring time and may reduce the variation of contouring among different specialists [47].

The auto segmentation process requires a reference CT (named atlas) which is used to perform DIR between the latter and the new CT. The deformation matrix resultant from this DIR is used to propagate the contours of the reference CT into the contours of the new CT [46].

It is also possible to use DIR to propagate the contours of the fixed image to the movement image applying DIR. The use of DIR as a method of contour propagation was evaluated by Hvid et al. This study concluded that automatic segmentation using DIR techniques when propagating the contours from CT to CBCT lead to acceptable Dice Similarity Indexes. Therefore making possible the use of these algorithms in clinical context of ART or IMRT [48].

Li X. et al., tried to evaluate the DIR for contour propagation between CT and CBCT in head and neck adaptive radiation therapy. They used ten intensity-based DIR techniques, including B-spline[c], and rigid registration to propagate the contours of the CT plan to treatment CBCT of 21 patients. The initial delimitation of structures of interest was performed using Eclipse®. The contoured structures were

[c] DIR performed by B-spline method was implemented using an open source DIR package, Elastix.

divided by bony and soft-tissue. To evaluate the agreement between propagated contours and the ones delimitated by the specialist, a Dice Similarity coefficient (DSC) percentage of error (PE) and Hausdorff distance (HD) were performed, [49]. Even though previous studies suggested that DIR strategies (B-spline included) were better at contour propagation than RIR methods, on this study DIR did not perform necessarily better than RIR. It was concluded that DIR performed better in bony structures than in soft-tissue structures, and for different regions of interest with different degrees of freedom throughout the treatment [49]. Although this study seems to take the advantages of DIR in contour propagation, it only used intensity-based algorithms, and that might be the reason why the results did not support the use of DIR over RIR [49]. This study also suggested care when using intensity-based DIR in low contrast organs. Perhaps the solution is to use hybrid DIR when contouring low contrast organs.

Thor M. et al studied DIR for contour propagation from planning CT to CBCT scans in prostate cancer RT. The registrations were performed using Multi-modality Image Registration and Segmentation application (MIRS v.1.0, Varian Medical System). They have shown improvements of using DIR instead of RIR to contour propagation of tumour and structures of interest. They also investigated quantitatively and qualitatively the DIR algorithm concluding that propagation of the contours was statistically more successful for prostate than for bladder or rectum [50].

2.1.2.7. Dose accumulation

As stated previously, on each fraction of EBRT, it is supposed to deliver a specific amount of dose to the patient. However, due to changes of anatomical structures or even position changes, the delivered dose may not be the previously planned [51]. Dose accumulation is one of the DIR applications: it allows the calculation of the actual delivered dose to the patient at each treatment fraction [38]. Studies such as [51] used DIR to evaluate the differences between the estimated and delivered dose, suggesting that this is an issue that cannot be ignored.

Several studies were performed to analyse dose accumulation between different image modalities or dose accumulation affection by breathing motion. Yan et al studied the accumulate fractioned dose in a deforming organ by using a biomechanical model which calculated the DVF from the CT plan to each daily CT image set, acquired immediately before or after the treatment. Each DVF as well as the planning dose distribution were used to estimate the dose distribution of a region of interest. This type of study allows the comprehension of the response of human organs to radiation and the true relationship between volume and dose. With these models, it is possible to optimize the individual treatment daily [38], [52].

Even though CBCT's are useful to make sure the patient is at the planned position, since acquisition requires less X-ray projections and lower beam intensities than a CT, the image sets can have low contrast, low signal-to-noise ratio and artefacts. This turns dose calculations using CBCT less accurate. The solution might be using DIR to deform the pCT to each daily CBCT, to calculate the daily dose. However it is important to state that those mentioned characteristics of CBCT's may harm the image registration process [53].

In 2003, Schaly et al. aimed to calculate the daily dose delivered to EBRT patients. The dose accumulation procedure included the use of DIR with a TPS (Thin Plate Spline) transformation model. In this procedure, they started by contouring the bony structures on the planning and treatment study (CT scans) to transform the patient coordinate systems. After calculating the planned dose, they aligned the isocentre of treatment planning to the coordinate system of each treatment study CT to re-calculate the planned dose distribution. The next step included the use of DIR (with TPS) to map treatment dose distribution back to the planning study. This study demonstrated the statistical significant differences between planned and delivered dose, enhancing the importance of calculation of the daily dose [54].

Moteabbed M. et al tried to validate a B-spline algorithm and evaluate the delivered IMRT dose based on DIR for prostate treatments. They acquired a CT (planning CT) and CBCT of a pelvic phantom and then deformed both images using two patient-based deformation fields. Afterwards, the pCT was deformed to the CBCT, creating a new CT image. The software used for DIR was *Platismatch*, an online available software, and a B-spline algorithm was used to achieve better registration quality. The process was repeated with full, half full and empty bladder. They then evaluated the geometry of the images by comparing voxel-based HU and vector fields, and for dosimetry evaluation, compared the plan on the original CT with the warped images and the dose volume histograms of the similar warped structures in both images. This study concluded that it is feasible and accurate to use DIR on deformed planning CT to evaluate IMRT daily dose on patients with prostate cancer [55].

In order to study adaptive RT in head and neck patients, Veiga et al. studied in 2014 and 2015 the feasibility of dose of the day calculations using CT-to-CBCT deformable registration [56] and the uncertainties in dose warping due to choice of deformable registration algorithm [57]. All the studied patients in both studies acquired a planning CT (pCT) and CBCT's acquired at treatment day. On the first study, they used a B-spline Free Form deformation algorithm of *NiftyReg*, to deform the planning CT to each daily CBCT acquired at treatment position. Subsequently, they calculated the daily dose at each deformed pCT (D_{DIR}), the dose in a rigidly aligned pCT (D_{RIG}), the dose of a calibrated CBCT (D_{CBCT}) and the dose of a re-plan CT (D_{rCT}). The dose was calculated using Eclipse® (Varian Medical Systems). By comparing D_{DIR}, D_{RIG} and D_{CBCT} with the gold-standard D_{rCT}, this study lead to the conclusion that calculating "dose of the day" by deforming a pCT to the daily CBCT is possible, without need to acquire a new CT since the dose differences were clinically acceptable and D_{DIR} was closer to D_{rCT} than the other calculated doses [56]. After the first study, the group compared four different DIR approaches available in *NiftyReg*, to find the uncertainties in dose warping. They first mapped the HU information from pCT to each CBCT using DIR. Then, calculated the dose of the day on each deformed pCT and mapped the dose of the day back to the space of the pCT. The final step was to accumulate and display the dose distributions on the pCT space. The investigators compared four different approaches to dose warping and then concluded that different choices of DIR algorithms have larger impact in terms of dose warping in regions were the dose gradient is high and/or the image quality is poorer [57].

A study by Fusella et al (2016) used Velocity® for DIR to evaluate if the need for planning recalculations in deformed anatomies. Additionally, the authors aimed to find a way of using this DIR efficiently when applying it to dose warping: dose accumulation (DA) for Adaptive Radiation Therapy (ART)[d] and dose summation (DS) for re-treatment[e]. Dose mapping of different CT sets was performed using B-spline based registrations, and then validated by a set of 3 computational phantoms. On each phantom, they simulated both ART and re-treatment, to recreate clinical needs, and then performed DIR to find the displacement vector (DVF) for dose applications. Both deformed and recalculated doses were then compared. Even though this study validated the warping dose process obtained by registering various sets of images, they concluded that dose recalculation of the deformed images, seems to be a better solution for dose accumulation purposes and for image guided radiation therapy applications. This study emphasises the need of validating DIR algorithms, for applying it to clinic, and also the benefits of using this technique [45].

In 2017, Poon et al evaluated the deformed image-based dose calculations for ART nasopharyngeal carcinoma. Considering that current CBCT scans have less quality than CT images, they suggested the deformation the CT plan dose to each CBCT of RT sessions of patients with nasopharyngeal cancers

[d] Adaptive Radiation Therapy – Before any RT treatment fraction, the plan is re-evaluated and changed if needed, turning it into a systematically monitored treatment, where several factors are considered to optimize the treatment at each fraction.

[e] Re-treatment happens when it is impossible to find the planned position of the patient and is necessary to re-plan the whole treatment, taking into account the given fractions until then.

(NPC). The researchers used MIM software Inc, to execute image registration, applying a constrained intensity-based free-form registration algorithm for CT-CT. Then, calculated dose using Eclipse®, Version 10.0. The dose calculation of the deformed planning CT resulted in significant dose uncertainties in target volumes and organs at risk. They concluded that the deformable registration error was probably the cause of dose deviations found in OARs and target volumes [30]. Even though this study suggests that it is not feasible to use DIR for dose accumulation calculations, there are other studies that support this procedure.

Vickress J. et al, studied the impact of DIR errors in dosimetry and concluded that errors in DIR are inevitable when the objective is to obtain highly accurate DVF solutions. This group compared deformed landmarks with the defined ones and calculated the landmark actual displacement error, which was defined as the gold standard and used to evaluate the dose-predictive power of various measures of DIR error. They calculated the range of dose uncertainty (RDU) by measuring DIR error, and stated that RDU is a parameter that can provide a useful representation of the impact of the DIR algorithm in dosimetry [58].

Orlandini L.C. et al compared the cumulative with the planned dose of image guided, IMRT of the prostate bed and studied the feasibility of adding dose tracking to routine workflow for RT. They concluded that using DIR (with software RayStation, RaySearch Laboratories) to deform the planning CT to the daily CBCT's and calculate the cumulative dose after this procedure was a feasible method, that could save up some time on clinic, and help the professionals to take some decisions in adaptive treatment [59].

Despite of different study results when testing DIR on dose calculations, it was decided in this dissertation project that it is viable to preform pCT-CBCT DIR and then proceed to dose calculation on the reshaped CT's, if the DIR result is satisfactory.

3. MATERIALS & METHODS

On this project, for dose calculations and for patients plan visualisation it was used Eclipse® (v. 13.6 1996-2015 Varian Medical Systems, Inc). For DIR purposes, it was used Velocity® (v. 3.2.1. 2004-2015 Varian Medical Systems, Inc). For statistical analysis, it was used RStudio (Version 2.1, February 1999 - Copyright (C) 1991, 1999 Free Software Foundation, Inc.)

3.1. STUDY CASES

3.1.1. TREATMENT PROTOCOL

At Champalimaud Foundation, since 2016 it is being implemented a new approach of treatment when treating patients with cervical or endometrial cancer, to avoid tumour recurrence. This study was approved by the ethical commission of the CF. The patients included in this dissertation take part of this clinical study.

After surgery or following the first EBRT treatment or adjuvant chemotherapy, brachytherapy is usually given to the patient to avoid tumour recurrence. However, this clinical study protocol proposes the use of VMAT Stereotactic body radiation therapy (SBRT) instead of brachytherapy, as suggested in previous work [60]. On SBRT high dose radiation to tumours is delivered (not on spine or brain) requiring body immobilisation or monitoring (in our case, using *Calypso Beacons* [61] and IGRT), since small movements can disturb the precision of dose delivery [62], [63]. The usual treatment method now performed at clinic is described below.

For treatment Planning, is acquired a spiral CT (120 kV, 360 mAs, 1mm slice thickness).

Before treatment, in order to guarantee monitoring of patients' position, it is acquired a CBCT (125 kV, 1080 mAs, Fan type half, acquired with full trajectory).

When it is possible to remove the tumour and uterus with surgery, there are two options of adjuvant treatment, depending on tumour type (Table 1.1, Table 1.2 and Table 1.3):

- Exclusive SBRT local treatment (typically 3 x [7-10.5] Gy), usually adequate for endometrial intermediate-risk or intermediate-high risk cancer patients.
- Initial pelvic EBRT treatment (23 x 2Gy) plus local SBRT boost (typically 3 x [5 - 7.5] Gy). This is adequate for endometrial high-risk cancer patients. Nevertheless, if it is a stage III tumour, the patient is also submitted to chemotherapy.

When it is not possible to remove the tumour with surgery, mainly in cervical cancer patients, EBRT with 23 x 2 Gy (with or without lombo-aortic lymph nodes) is firstly prescribed. This treatment is usually followed by SBRT boost treatment of 5 x [4 – 5] Gy. In these cases, weekly radiosensitizer chemotherapy is performed simultaneously with the EBRT and SBRT treatments, to improve locoregional control probability.

Before SBRT, a planning CT (pCT) of the patient is acquired. CT protocol requires full bladder (filled with 200 cc of serum and 15cc of iodine contrast), a brachytherapy vaginal cylinder (which has *Calypso beacons* for tracking [61]) and a rectal balloon (filled with 50 cc of air). An example of a 3fr patient pCT, whose uterus has been removed before SBRT is shown in Figure 3.1.

The radiation oncologist contours the clinical target and the "organs at risk" (OARs) volumes and the prescribes the doses to each target volume. Recommendation on OARs maximum doses are also prescribed. Then treatment planning is performed with Eclipse®.

The required contoured structures are the CTV (VC -Vaginal Cuff - and VCM - Vaginal Cuff Mucosa), PTV, rectal wall, urethral wall, sigmoid, small bowel, body, bladder wall, vagina, vaginal

cylinder, rectal balloon and ring structure. The physicists can also add structures named "CTV/PTV Calc/Calculation", "CTV/PTV + x mm" which guarantee the delivery of a specific amount of dose to these crucial areas, for planning purposes. The specific structure "Ring" is not an anatomical structure, and is created to avoid the excess of dose in the surrounding area of the PTV

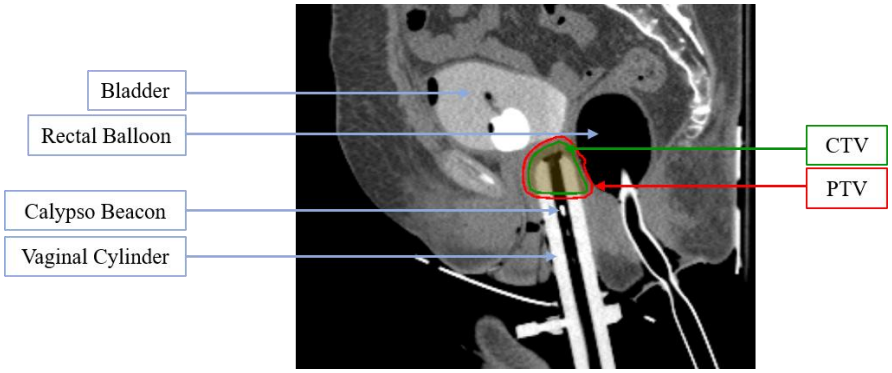

Figure 3.1: Sagittal view pCT of a 3x7.5Gy patient. CTV in green, PTV in red. Bladder, rectal balloon, beacon and cylinder shown in the figure.

3.1.2. STUDY PATIENT SAMPLE

We had a total of 49 gynaecological cancer patients in our database, treated with a local vaginal SBRT treatment to avoid tumour recurrence. Only 23 of the 49 were suitable for this study since the patients were excluded if:

- No vaginal cylinder or rectal balloon were present;
- The patient was not treated for cervical or endometrial cancer;
- A CBCT or spotlight CBCT did not have quality enough for contouring the relevant structures;
- The CBCT did not cover all the ROI's intended (vaginal cylinder, Rectal Balloon or Bladder and specially PTV). Given that the rCT resultant from these excluded patients result in an inadequate deformation.

From the 23 gynaecological cancer patients used for this study:

- 8 patients passed through 5 fractions of SBRT (5fr patients). These patients were not submitted surgery to uterus removal:
  - 7 patients (5x5Gy) – cervical cancer
  - 1 patient (5x4Gy) – cervical cancer. Patient received also 1x8Gy to iliac lymph nodes.
- 15 passed through 3 fractions of SBRT (3fr patients). These patients had their uterus removed:
  - 12 patients (3x7,5Gy) – high risk endometrial cancer
  - 1 patient (3x 7,5Gy) – cervical cancer, tumour surgically removed
  - 2 patients (2x10,5Gy) – intermediate risk endometrial cancer

3.2. VELOCITY®

3.2.1. DIR ALGORITHMS

Velocity® software allows choosing which type of objective function, depending on the image set conditions: it is possible to deform images based on pixel intensity or on image features. The software primary registration uses a multi-resolution approach and the objective function is based on Mattes Mutual Information (MI). MI allows measuring two random variables dependent on each other and it

quantifies the amount of information it is possible to obtain of one of these random variables from the other [64].

Even though Velocity® offers several registration algorithms, in this study only two were used. These algorithms are the most adequate to deform higher quality images (pCT scans) to less quality image sets (CBCT scans) [65]: CBCT corrected deformable (CD) and Structure Guided Deformable registration (SGD). Deformable Multi-pass (DMP) is another registration algorithm which was used only in the validation phase of this study. It is ideal for CT to CT registration, two high resolution scans [65].

CD is a three-pass deformable registration. It includes a CBCT filter and is suggested for CT to low noise CBCT registration [65]. SGD registration is a hybrid registration of the Deformable Multi-pass, which is influenced by the contoured structures of interest. The structures must be contoured manually on the moving and fixed images. This method is useful in cases where the deformation is difficult due to dramatic changes (eg. the bladder can suffer a lot of changes between fractions of treatment), and requires the use of Navigators Velocity® feature [65].

As a transformation model, Velocity® software uses a cubic (order 3) B-spline model in order to maximize the similarity index between the moving and fixed image [44].

On Velocity®, grid size and limitation of the registration space to a region of interest is configurable to allow the optimization of the settings of registration parameters. In order to guide the user to some tasks step-by-step. Navigators feature guides the user step-by-step in some tasks, like SGD DIR for example.

3.2.2. DEFORMATION PROCESS

The objective was to deform a pCT into a CBCT by using DIR on Velocity®, so we started by choosing the pCT as the fixed image and the CBCT as the moving image. Which means that on Velocity®, the pCT was chosen as the primary image and the CBCT as secondary.

In clinical practice, the rigid registration is performed and approved by the radiation oncologist before treatment. In order to apply the SGD DIR, contouring of relevant structures had to be performed (on CBCT and pCT) (Chapter 3.2.1).

To compare different rCT's coming from the same pCT-CBCT registration, it is needed to have the same ROI of DIR. Therefore, hybrid registration (SGD) was performed firstly. Then, the SGD DIR ROI was conserved and was performed deformable image registration intensity-based (CD), without need of using Navigators[f]. The ROI had to include the whole PTV region, bladder and rectal balloon, and the cylinder as shown in Figure 3.2.

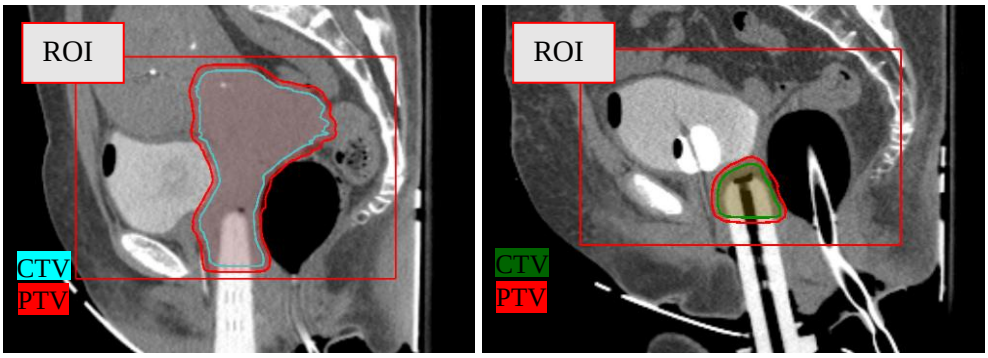

Figure 3.2: 5fr patient DIR ROI (left) vs 3fr patient DIR ROI (right)

[f] To perform DMP DIR, there is no need of using Navigators. It is a similar process to CD DIR.

Then, Velocity® supplied the two deformation matrixes (which transform the CBCT on the pCT) resultant from the two DIR processes.

After, we found the inversed matrixes (which transform the pCT on the CBCT), in order to created two planning **reshaped CT's** (CD rCT and SGD rCT). These have the image quality of a CT scan, but are similar to the correspondent CBCT.

3.2.3. QUALITY ASSURANCE (QA) AND VALIDATION OF VELOCITY®

Velocity® uses a modified cubic B-spline deformable registration algorithm with MI-based matching. To make sure the DIR is correctly performed, any user of this software can choose between three options: 1. Assess tissue/voxel intensity overlay – allows the observation of the deformed and original images, at the same time ; 2. Assess the deformable warp map – gives us the visual representation of voxel displacement from the original to the deformed image; 3. Display the difference map between two registered images [65]. This quality assurance method is a qualitative method.

To perform a quantitative evaluation, a conformality tool that allows the comparison of two structures can be used. This Dice Coefficient of Similarity (DSC) measures the similarity of two structures [0 (no similarity) to 1 (identical structures)] by comparing the overlapped volume [65].

Qualitative and quantitative evaluation methods were used in this project to classify each deformation.

To assure that Velocity® does not damage image quality, leading to misrepresentation of dose calculation, the software validation was initiated with the deformation of a pCT on itself, using both CD and SGD methods and another method known as Deformable multi-pass, which is indicated for CT-CT deformations. It was chosen the pCT of an endometrial cancer patient, submitted to 3 x 7.5 Gy of VMAT SBRT.

Using Velocity®, it was created a copy of the chosen patient pCT named "pCT scaled". After, it was selected the pCT as the fixed imaged and the pCT scaled as the moving image. Then, it was performed CD, SGD and DMP DIR. The whole body was chosen as the ROI for deformation. Were created three reshaped CT's resultant from the DIR, and the propagated contours were compared with the original contours using Velocity's conformality tool. The created rCT's were then exported to Eclipse®. After, the original plan was copied to the rCT's and then it was calculated the dose on the rCT's and posteriorly compared with the planned dose on the pCT.

Subsequently, were compared (between each rCT and the pCT) on Eclipse® the values of Volume, minimum, maximum and mean dose of the original plan and the plan of the structures on the rCT's named CD (CBCT corrected deformable), SGD (Structure guided deformable) and DMP (deformable multi-pass).

Volume variable measures the volume of a contoured structure in cm^3. Minimum, maximum and mean dose (in Gy), measure the minimum, maximum and mean dose delivered to a specific contoured structure.

It was calculated the percentage error of every structure between the value of each variable (x) measured in the pCT and in the rCT's:

$$\text{Error } (\%) = \frac{\left|x_{pCT} - x_{rCT}\right|}{x_{pCT}} \times 100\% \qquad (3.1)$$

The previous procedure was repeated but acquiring a copy of the pCT on Eclipse®, which was exported to Velocity® to perform DIR.

Since the global evaluation of abdomen and pelvis DIR using Velocity® is not easy due to all non-rigid structures, it is important to verify the accuracy of the software. For this reason, it was performed DIR in Head and Neck CT and CBCT scans which are scans have more rigid structures surrounding and DIR results in higher quality rCT's. Also, it was performed DIR in prostate CT and CBCT scans, which are more similar to the study cases, allowing the evaluation of DIR in cases similar to the studied on this dissertation.

The Head and Neck patient chosen was diagnosed with nasopharyngeal cancer and for treatment passed through 33 x 2.121 Gy EBRT. Were created six reshaped CT's from the 2nd, 6th, 23rd ,24th ,25th and 33rd CBCT acquired in the correspondent fractions of treatment. We only performed the CD DIR, and then classified the reshaped CT's considering only the PTV area. To evaluate the deformation of this case, it is possible to only use qualitative evaluation, since it is an area surrounded by bone.

The prostate cancer patient chosen was submitted to 28 x 2.5 Gy of EBRT. Were created 2 rCT's, by using DIR, correspondent to the 1st and 28th CBCT acquired during treatment. For this study case, it was performed only intensity-based DIR (CD on Velocity®) since as suggested in Velocity® user manual, SGD is useful as an alternative to the last type of registration when achieving non-satisfactory results. Since the radiation oncologist is the only one capable of identifying the structures on CBCT's and reshaped CT's, he contoured the bladder, CTV and Rectum of the reshaped CT's twice (with one month apart) and contoured the same structures on the correspondent CBCT's. The propagated contours of the bladder, CTV and rectum were acquired by using the deformation matrix to deform the correspondent contours on the planning CT. After it was calculated the conformality between the contours made by the specialist and the propagated contours on CBCT's and rCT's, to analyse deformation quality.

3.3. DEFORMATION AND CLASSIFICATION PROCESS FOR THE STUDY CASES

The image deformation process for our study cases using Velocity®, started by contouring at each CBCT and at the pCT the bladder, cylinder and rectal balloon[g]. In some patients, bladder, cylinder and rectal balloon had already been contoured by the radiation oncologist at the pCT After performing both DIR processes, we had two rCT's with image quality of a CT scan but similar to the correspondent CBCT.

By comparing the CBCT's anatomy structures contours and correspondent structures on the rCT's of all patients, was classified qualitatively the deformation of the Bladder ($c_{Bladder}$), Cylinder ($c_{Cylinder}$) and Balloon (c_{Ballon}). The classification scale was: 1 - Bad, 2-Medium and 3-Good. Depending on the combination of the classifications of the structures of interest (c_1,c_2 and c_3), the rCT's were included in distinct groups of classification, I to VII (worst to best level of classified rCT). The rCT was considered approved for dose calculation if included in group VI or group VII. Table 3.1 represents the classification of the rCT's depending on the classification of the structures of interest.

[g] This contouring allows the hybrid deformation. The feature-based image registration is based on the contours of the same structures on the moving and fixed image.

Table 3.1: rCT classification.

c_1	c_2	c_3	rCT Classification (I – Worst … VII – Best)	rCT Approval (1 – Yes | 0 – No)
3	3	3	VII	1
3	3	2	VI	1
3	3	1	V	0
3	2	2		0
3	2	1	IV	0
2	2	2		0
3	1	1	III	0
2	2	1		0
2	1	1	II	0
1	1	1	I	0

For the first ten patients, the rCT classification was made considering all the ROI deformed and afterwards it was decided to consider the PTV region. The comparison of these two classification methods was performed using R Studio. The method of considering only the PTV region for classification, was approved by the radiation oncologist specialist on gynaecological cancers.

In Figure 3.3 is shown the deformation and classification process of a 3-fraction SBRT treatment patient, which is analogous to a 5-fraction SBRT treatment patient.

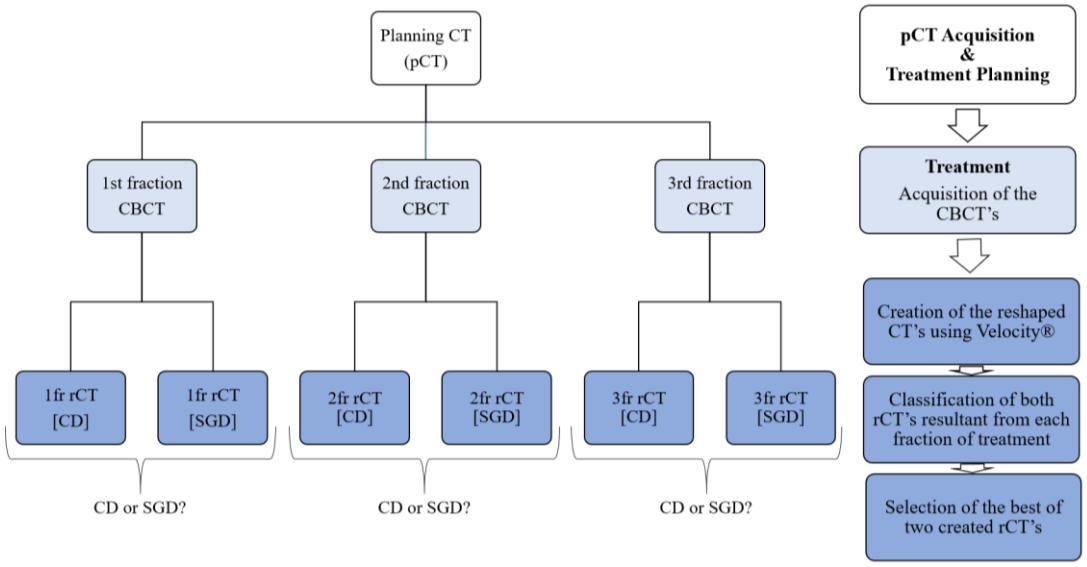

Figure 3.3: DIR process of a 3-fraction treatment patient.

As a complementary method for qualitative classification, Velocity's conformality tool was used. The values of conformality between the CBCT contoured structure and the one propagated structure created on the rCT were acquired ($conf_{Bladder}$, $conf_{Cylinder}$ and $conf_{Balloon}$). The mean value of conformality ($m_{conformality}$) was obtained by:

$$m_{conformality} = \frac{conf_{Bladder} + conf_{Cylinder} + conf_{Balloon}}{3} \quad (3.2)$$

3.3.1. COMPARISON OF TWO DEFORMATION METHODS

The deformation method more adequate to these patients was obtained by comparing the results of qualitative classification and the conformality values of the same structures. Resulting from CD and SGD deformation, it was aimed to decide which deformation method was more adequate for these patients.

The comparison was performed by using R Studio.

3.3.2. COMPARISON OF THE RESHAPED CT'S OF PATIENTS WITH OR WITHOUT UTERUS

From chapter 3.1., it is known that patients treated with a 3-fraction SBRT, contrary to 5-fraction patients, had their uterus surgically removed, to eliminate the tumour (totally or partially).

We had a total of 40 CBCT's from the patients whose uterus had not been removed while 45 CBCT's from patients whose uterus had been removed. This resulted in a total of 40 rCT's (CD and SGD) from 5fr patients and 45 rCT's (CD and SGD) from 3fr patients.

As shown in Figure 3.4 and Figure 3.5, the presence of the uterus in the 5fr patients provides a larger restraint in the surrounding organs. Besides, in Figure 3.5 is illustrated that the differences in contrast between the uterus and the surrounding organs (not including the bladder, balloon or cylinder) are not very significant. Poor contrast, and the larger PTV region, are facts that may contribute to differences in quality of the rCT's.

Since the conditions of the patients are not identical, was also addressed the influence of these different conditions in the DIR process.

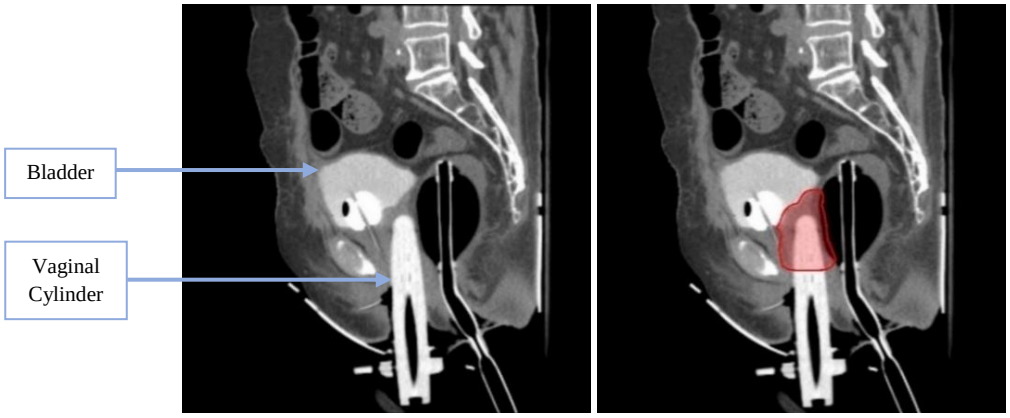

Figure 3.4: pCT sagittal view. Patient **with no uterus**. On right, PTV region in red.

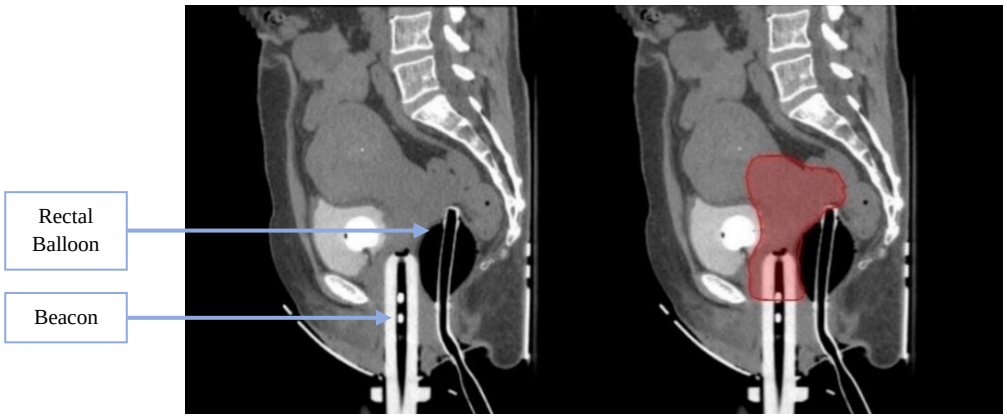

Figure 3.5: pCT sagittal view. Patient **with uterus.** On right, PTV region in red.

3.4. DOSE CALCULATION

After obtaining the reshaped CT's of all fractions of treatment, the next step was to calculate the actual delivered dose to the patient.

The best case was to have at least one approved rCT between the two created at each fraction of treatment, so that it was not needed to replace it by another fraction rCT. The best qualitatively classified (Table 3.1) of each pair of rCT's was chosen and then exported to Eclipse® (in Figure 3.6, the rCT chosen is marked with the blue "x"). In case of the same qualitative classification, the rCT with the highest $m_{conformality}$ was exported.

In case there was a fraction of treatment not having an approved rCT, the rCT chosen to replace that missing rCT was the one with the worst qualitative classification, to observe the "worst case scenario".

The delivered treatment was copied to the sum plan of all the exported rCT's and the dose map was calculated and superimposed on the planning CT. In this way, the dose was visually assessed in the coordinate system of the pCT – this was named SD (Sum Dose). The dose was calculated on the rCT's by copying the delivered plan weighted with the dose per fraction. This first step aimed to evaluate the deformation magnitude and to prepare the following step back to Velocity®. Subsequently, the dose maps of each fraction rCT were exported to Velocity® and were deformed applying the deformation matrixes between the rCT and the pCT. Then, the total deformed dose map, was calculated by adding all the dose maps, correspondent to each fraction of treatment. This was named actual delivered dose (ADD). An example procedure is visualised on Figure 3.6.

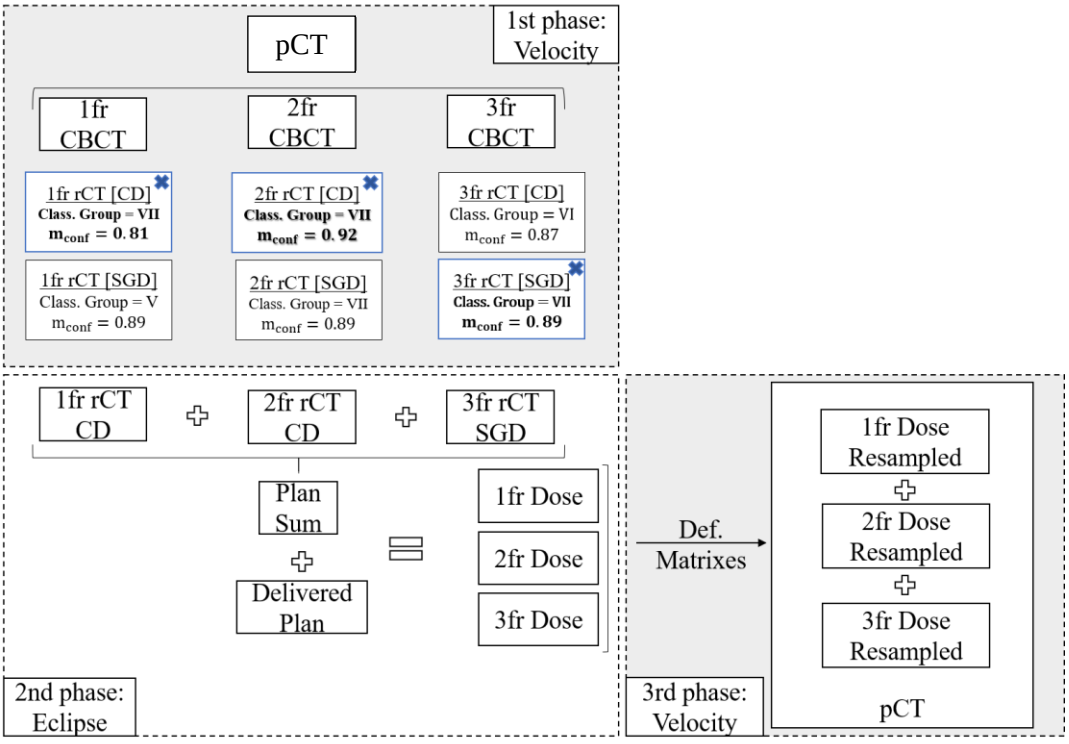

Figure 3.6: Example of process from the image deformation until the dose calculation where all the fractions (fr) of treatment had an approved reshaped CT (rCT). 3 fraction SBRT patient.

The delivered dose to the small bowel, rectal and bladder wall was analysed, since these are organs at risk which are evaluated by the radiation oncologist when approving the delivered patient plan. It was also acquired the total percentage of delivered dose to the PTV and CTV.

4. RESULTS & DISCUSSION

4.1. VELOCITY®: VALIDATION

Before proceeding to DIR on the available scans of our study cases, a test was conduct in Velocity®. The effects on dose calculation were analysed on a CT deformed on itself and by analysing DIR on a head and neck and on one prostate cancer case.

4.1.1. DIR – PLANNING CT

As described previously on chapter 3.2.3, the pCT was firstly copied on Velocity® creating the "pCT scaled" The pCT was settled as the fixed image and the "pCT scaled" as the moving image, and were created three rCT's by performing DIR, using the three following registration algorithms: CD, SGD, and DMP. For each rCT were acquired the propagated contours, by applying the resultant deformation matrixes on the pCT contours.

First, the pCT was compared with created rCT's, using the spyglass tool of Velocity®. By evaluating qualitatively, the rCT's were equal to the pCT, as expected. On Figure 4.1, Figure 4.2 and Figure 4.3, it is possible to visualise the three rCT's created above the pCT and it is easy to confirm that the images are similar.

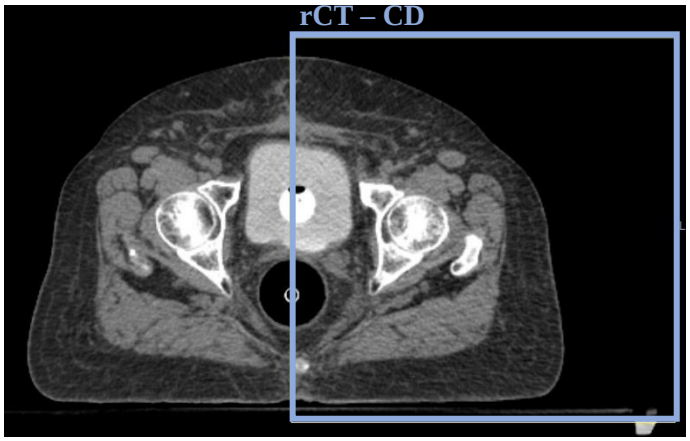

Figure 4.1: Axial view of the pCT below the rCT (CBCT Corrected deformable – surrounded in blue).

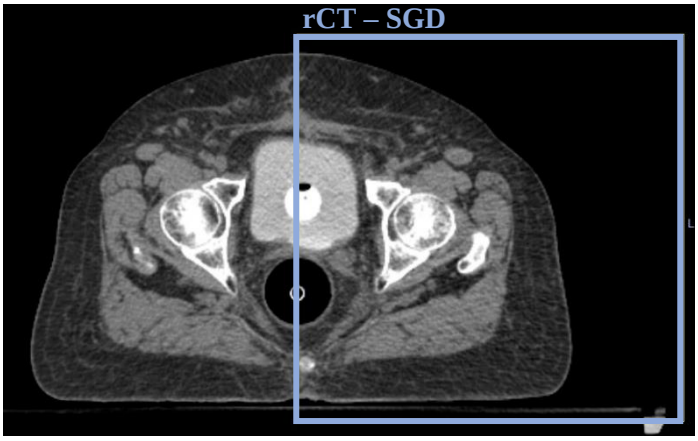

Figure 4.2: Axial view of the pCT below the rCT (Structure guided deformable – surrounded in blue).

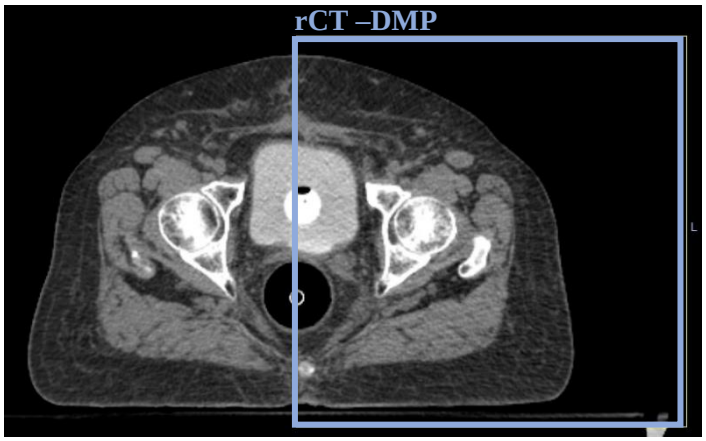

Figure 4.3: Axial view of the pCT below the rCT (Deformable multi-pass – surrounded in blue).

Since the moving and fixed image were the same, when performing DIR, as expected were generated three null deformation matrixes, which would theoretically result in propagated contours equal to the contoured on the pCT.

The next step was to compare the automated contours on the rCT's with the correspondent ones on the pCT, by using the conformality tool. The structures of the pCT were: rectal balloon, bladder wall, body, bowel small, CTV (VC, VCM and + 5 mm), right and left femur, PTV (Calculation and VC), rectal wall, ring, sigmoid, urethral wall and vagina. The conformality between the propagated contours (of all rCT's) and the correspondent contours of the pCT was always **1** according to Velocity®. This indicated the nullity of the deformation matrixes which was then confirmed.

As is it possible to visualise in the following boxplots (Figure 4.4, Figure 4.5,Figure 4.6 and Figure 4.7) we can firstly verify that there are no differences in the errors between the different rCT's, indicating there are no differences between the three generated rCT's (N=16).

When analysing the volume of different structures (Figure 4.4) it is observed that there are structures in the rCT's that present from 0.0% to 4.4% difference in volume from the pCT. The median is positioned in a 0.4% difference, the mean error value is 0.8% and the standard deviation is approximately 1.1%. The fact that the median is positioned at 0.4% indicates that more than 50% of the sample presented an error inferior to 0.4%. The structures that presented the largest error in volume were Urethral Wall (4.3%) and the "PTV calculation" (2.2%). CTV VCM also presented an error superior to 1%. These differences in volume, were not observed in Velocity®.

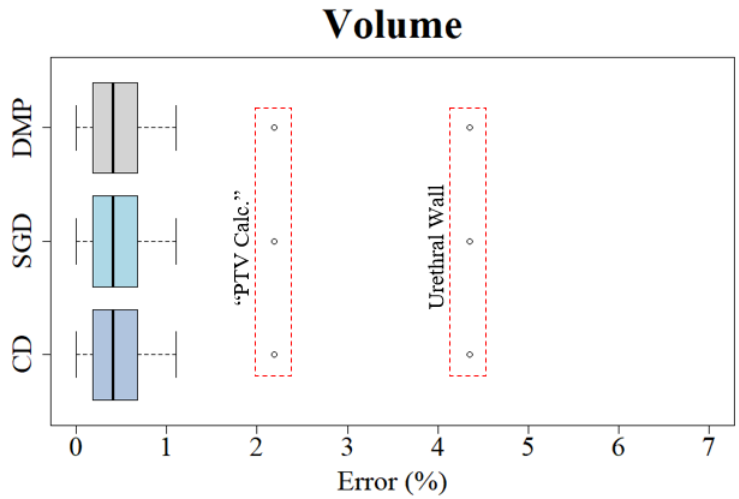

Figure 4.4: Percentage **volume error** between the structures on the pCT and the rCT's [CD, SGD and DMP]. "PTV Calc" and Urethral Wall errors represented surrounded in red.

The distribution of percentage minimum dose errors on the structures of the pCT and the structures of the rCT's (N=16) is shown in Figure 4.5

The median is positioned at 0.0%, and the standard deviation is 2.0%. The mean value is 0.9%. Ring presented an error of 6.6%, "CTV+ 5 mm" presented an error of 5.0%, and "PTV Calculation", PTV, CTV VCM presented an error of 1.0%. The remaining presented a 0.0% error. When the error was superior to 0.0%, the value on minimum dose was always higher in the rCT's than in the pCT.

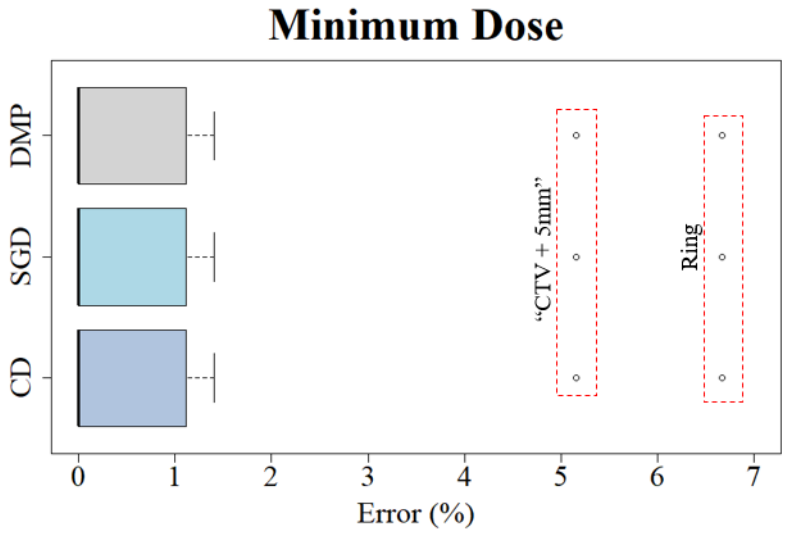

Figure 4.5: Percentage **minimum dose** error between the structures on the pCT and the rCT's [CD, SGD and DMP]. "CTV + 5 mm" and "Ring" errors represented surrounded in red.

Figure 4.6 shows the distribution of percentage maximum dose errors between the structures on the pCT and the rCT's (N=16). The median is positioned at 0.0%, the standard deviation is 0.2% and the mean value is 0.1%. Only the rectal wall, ring and urethral wall presented an error superior to 0.0%. The rectal wall had a maximum dose value on the rCT's higher than on the pCT's and the rest had a lower value.

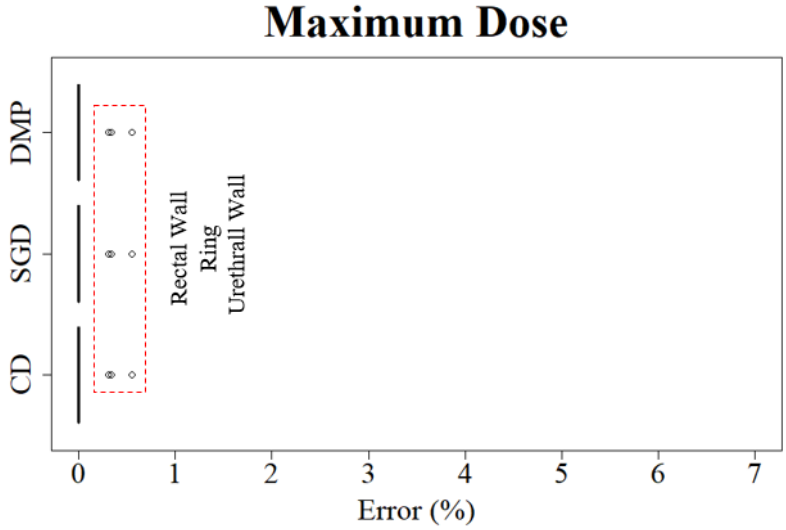

Figure 4.6: Percentage **maximum dose** error between the structures on the pCT and the rCT's [CD, SGD and DMP]. Rectal Wall, "Ring" and Urethral Wall errors represented surrounded in red.

On Figure 4.7 is possible to analyse percentage mean dose error between the structures on the pCT and the rCT's. The median is positioned at 0.0%, the standard deviation is 0.6% and the mean value is 0.3%. The structures that presented an error superior to 0.0%, even though inferior to 0.3% were, CTV VC, "CTV + 5 mm", "PTV calculation", PTV VC, Urethral wall and vagina. The structure with the highest error (2.2%) was the Bladder Wall.

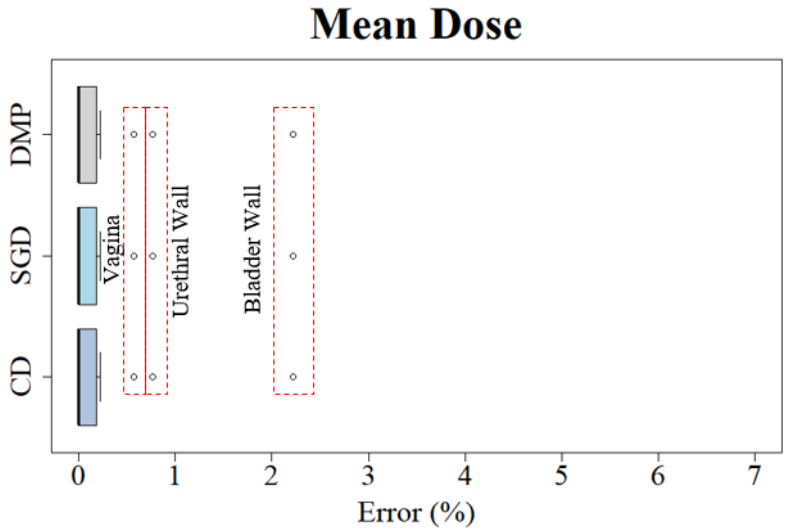

Figure 4.7: Percentage **mean dose** error between the structures on the pCT and the rCT's [CD, SGD and DMP]. Vagina, Urethral Wall and Bladder Wall errors represented surrounded in red.

There should be no differences between the measurements of the original plan and the calculated plans with the rCT's, since the rCT's are similar to the pCT. This was suggested when analysing the deformation matrix and the conformality between structures in Velocity®. However, when analysing the rCT plans on Eclipse®, errors were observed in the volume of structures, minimum, maximum and mean dose. There was not a consistency in the structure that presented errors.

The previous results suggested that an error was introduced in the whole process, and it is visible when the doses are calculated on Eclipse®. There were possible reasons that justified this error such as the exportation and importation of scans on Velocity® and Eclipse®, the pCT copy on Velocity®, or even the deformation process on Velocity®.

In order to find the error source, it was exported to Eclipse® the scaled CT, and then the original plan was copied to the scaled CT for dose calculations.

The measured errors of all the variables previously analysed were all equal to the errors measured on the three rCT's indicating that the error was not introduced during the deformation process.

Due to these outcomes, instead of creating a copy of the pCT on Velocity®, it was created a copy on Eclipse® (pCT copy), which was then exported to Velocity® to repeat the process and to try to find the source of errors.

On Velocity®, the pCT was chosen as the primary image and the pCT copy as the secondary and were created three rCT's using three different DIR processes: DMP, CD and SGD. As in the previous case, Velocity® showed a null deformation matrix for the three rCT's. Then, it was checked if the conformality between the second rCT's structures and the pCT copy structures was 1. This value was 1 between all the correspondent structures, making it possible to keep with the previous procedure of dose calculation.

The second rCT's, as well as the correspondent propagated structures were exported to Eclipse®. The original plan was copied to each of the second rCT's and then dose calculation was prepared on those and on the copy pCT.

There were found no differences between the copy pCT doses and the original plan. Nevertheless, the errors found between the original plan and the second rCT's were equal to the errors found between the plan and the firstly created rCT's (from the scaled CT).

The copy pCT, after being imported to Velocity®, was then again exported to Eclipse®, where we calculated again the delivered dose on this scan. This exported and imported copy pCT showed now differences from the original plan doses, which were similar to the previously found errors.

This data lead to conclude that the differences between the original plan and the rCT's plan are probably due to small modifications introduced by the filters when importing images to Eclipse®, and different filters are not accessible in this software.

The larger percentual differences were noted in the lower volume structures, even though in exact number, the differences were minimal.

When in the next chapters we calculate rCT's delivered dose is necessary to consider the slight changes in the HU of the scans, introduced by the importation of images to Eclipse®, which may result in small errors in dose calculation.

4.1.2. DIR – HEAD & NECK

The second phase on this validation process was to test DIR on a head and neck (H&N) case which is usually a simpler process and has better results than on abdominal-pelvic region scans, due to the larger presence of bone structures.

Acquired rCT's from our H&N case were qualitatively classified with levels 1 (bad), 2 (medium) and 3 (good), when compared with the correspondent CBCT's. A well classified rCT had the contours of bones and other structures matching the ones of the correspondent CBCT.

For classification, it was considered only the PTV region only. From the six rCT's created (correspondent to the 2nd, 6th, 23rd ,24th ,25th and 33rd fractions of treatment), only one presented medium classification while the rest had a good classification.

From these data, it is possible to affirm that the software can perform satisfying DIR at least with cases where the rigid regions are predominant. This can be explained by the fact that the intensity-based DIR process is more efficient when facing higher differences in intensity such the existent in the H&N scans. The craniofacial bones have higher HU (+200 HU at craniofacial bone at CT) and white and grey matter and the other structures in head have HU intensity lower than +45 HU (HU intensity of different structures is clarified in Figure 4.8). Clear contours of these images are generated by this high contrast between different structures.

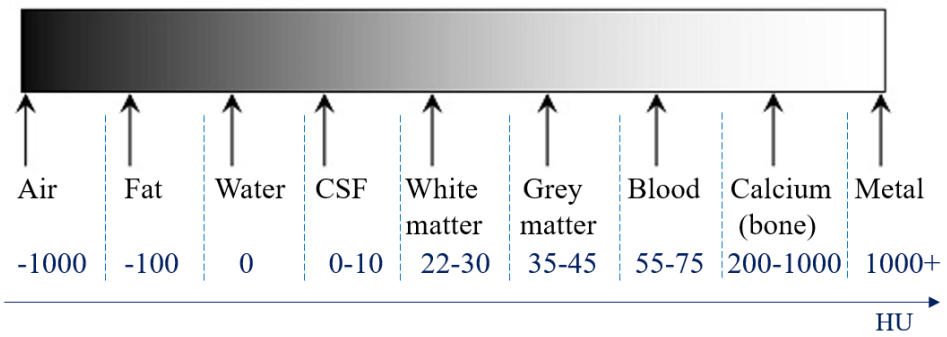

Figure 4.8: HU scale according to different substances. Only applied to CT scans, not to CBCT.

The fact that the linear attenuation coefficient is meaningfully different between different head and neck structures, makes the scans as clear in a CT as in a CBCT (Figure 4.9**),** independently of the lower quality of CBCT. However, it is always noticeable the lower quality of image of CBCT scans**.**

For the reasons explained previously, and since the CBCT corrected deformable is an intensity-based DIR method of Velocity®, these significant differences in intensity between diverse structures facilitates the match compared to DIR on an abdominal-pelvic region.

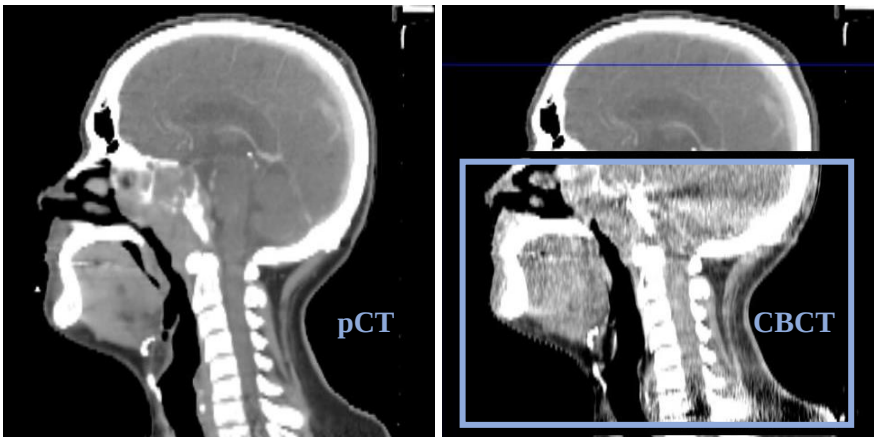

Figure 4.9: Planning CT (pCT) of the Head and Neck study case on the left and the 2nd fraction of treatment CBCT on top of the pCT on the right.

Classifying H&N rCT's is basically compare the bones on CBCT and rCT, which is a simpler process than classifying abdominal-pelvic rCT's. Without having completed DIR on the case above (2nd fraction of treatment), it is noticeable that the planning CT and the CBCT are similar, which indicates that only slight changes may be needed on the pCT to approach CBCT.

On Figure 4.10, the result of the DIR applied to the images of Figure 4.9 is shown: the 2nd CBCT and the correspondent rCT are very similar. The rCT is above the CBCT, represented surrounded by the blue line.

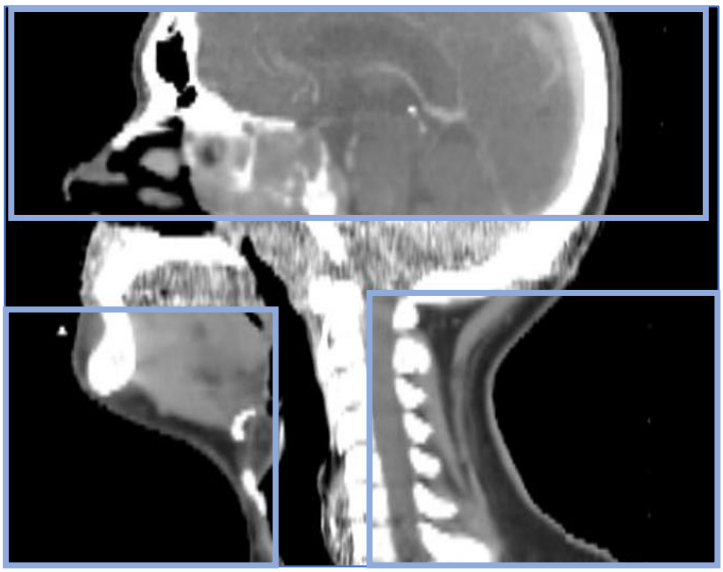

Figure 4.10: 2nd fraction CBCT below the correspondent rCT (surrounded in blue).

Figure 4.9 and Figure 4.10 is another example of a successful and simple DIR process. The CBCT was already similar to the pCT, so the deformation matrix despite not having a significant impact, was enough to turn the pCT on a perfect "copy" of the CBCT.

Not every DIR process was as simple as the last one. When acquiring a H&N pCT or CBCT, the degrees of freedom that can create differences between both are mainly due to neck position. This is the reason why occasionally the existent differences between the pCT and CBCT's are usually in this region, as it is visualised in Figure 4.11, which corresponds to the 23rd fraction of treatment CBCT of the same patient. On Figure 4.11, the CBCT is surrounded in blue, and above the CT. The arrows indicate the regions with larger difference between the two scans.

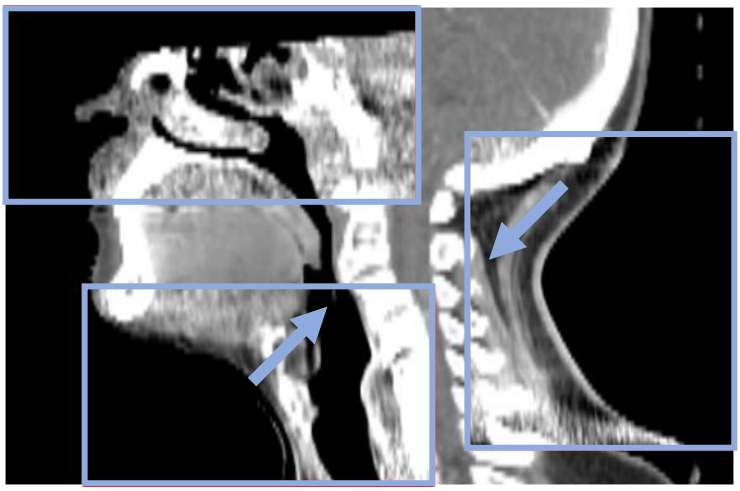

Figure 4.11: 23rd fraction CBCT (in blue) above the planning CT.

On Figure 4.12 we can verify that when the pCT was reshaped into the form of the CBCT, the images match almost impeccably such as in Figure 4.10. The CBCT structures now match the rCT, contrary to Figure 4.11 where there were significant differences in the neck region.

Figure 4.11 and Figure 4.12 show an example of a successful case of deformation of the planning CT to the form of the CBCT.

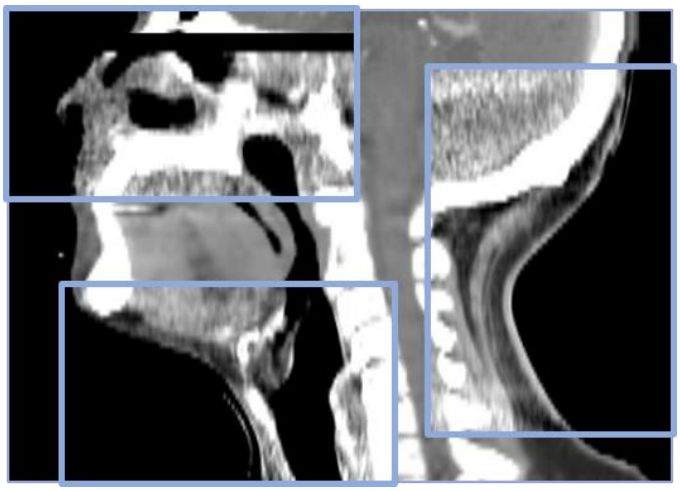

Figure 4.12: 23rd fraction CBCT (in blue) above the rCT.

The analysis of the deformation of the H&N images confirms the good performance of the software when using **intensity-based DIR**. Since these were simple cases, the deformation using only intensity-based DIR was enough to achieve satisfactory results.

We did not proceed to dose calculations to check if the planned dose was the delivered, since the objective was only to prove the reliability of Velocity® when performing DIR intensity-based.

4.1.3. DIR – PROSTATE

The data from the prostate cancer analysis is a comparison between the contours made by the radiation oncologist on the rCT's and on the CBCT's and the propagated contours resultant from the deformation matrix when applied to the contours of the pCT, allowing the evaluation of deformation quality.

Velocity's conformality tool was used to compare the contours. Below, on Table 4.1 and Table 4.2 it is possible to analyse the summarized acquired data.

Table 4.1: Conformality between the contours drawn by the radiation oncologist on the reshaped CT with a month apart (Contour I and Contour II), the propagated contours (Contour CD) and the CBCT contours **[1st fraction rCT].**

	Conformality					
	Contour I vs Contour CD	Contour II vs Contour CD	Contour I vs Contour CBCT	Contour II vs Contour CBCT	Contour I vs Contour II	Contour CD vs Contour CBCT
Bladder	0.95	0.95	0.79	0.79	0.96	0.79
CTV	0.87	0.88	0.92	0.90	0.93	0.88
Rectum	0.88	0.92	0.87	0.85	0.92	0.82

Table 4.2: Conformality between the contours drawn by the radiation oncologist on the reshaped CT with a month apart (Contour I and Contour II), the propagated contours (Contour CD) and the CBCT contours **[28th fraction rCT].**

	Conformality					
	Contour I vs Contour CD	Contour II vs Contour CD	Contour I vs Contour CBCT	Contour II vs Contour CBCT	Contour I vs Contour II	Contour CD vs Contour CBCT
Bladder	0.96	0.96	0.82	0.81	0.97	0.82
CTV	0.86	0.90	0.87	0.88	0.91	0.87
Rectum	0.86	0.89	0.92	0.86	0.90	0.84

The values of the 5th column of both Table 4.1 and Table 4.2 allow the comparison between the contours in the rCT made by the specialist in two different times. The fact that the values are all above 0.90 indicates that the completed contours had a similar shape even though the difference of time. Also, the fact that the conformality between contours I and II (column 5) is above 0.9 but not 1 on both tables gives support to the theory that on the rCT the structures as visible enough to contour it well. Also, even though the conformality between two similar structures is not 1, it does not mean that the contours are not similar. It indicates the difficulty of contouring structures using only the CT scans. This was already discussed on previous literature: the contouring of same structures by different specialists, or by the same specialists on separated times, using only CT scans can result in higher variations of contouring

than when the same structures are contoured using not only CT scans but also other imaging methods such as PET [66].

The values of the conformality of the rectum on Table 4.2 on column 3 and 4 are the ones that differ the most, and the conformality between rectum contour I and II on the rCT is the smallest within the three on both tables. The challenge faced when contouring the rectum, and the low quality of the CBCT's are two reasons that explain this fact.

Also, the fact that the values of columns 1 and 2 are all higher than 0.85 indicates that the propagated contours created by the deformation matrix are similar and correspond to the structures visualised by the specialist on the rCT, validating propagated contours.

Column 6 of both Table 4.1 and Table 4.2 allows the brief quality evaluation of intensity-based DIR (CBCT Corrected Deformable). The larger the conformality between the contour of a structure on the CBCT and the same structure propagated, the larger quality of the rCT when compared with the CBCT, which implies a better result of DIR. As it is going to be described on the following chapters, in some cases, conformality of 0.8 between the reshaped structure and the one contoured on the CBCT, is an indicator of a satisfying result of DIR. As it is possible to see on Table 4.1 and Table 4.2, the conformality between the rCT propagated contours and the CBCT contours and rCT is always above 0.80. This is an indicator that the application of DIR on these prostate cancer cases was successful, and that in result were created two rCT's similar to the correspondent CBCT's of treatment.

As it is going to be discussed in the following chapters, even though conformality is not a 100% reliable predictive tool for a good DIR result, it may be a tool to help classifying a rCT resultant from CD DIR.

This prostate cases rCT's analysis, shows that the software can work properly when the ROI of the applied DIR has predominance of soft structures such as rectum or bladder. This first phase of the study allowed to proceed with Velocity® on cervical and endometrial cancer scans.

4.2. RESHAPED CT'S ANALYSIS

4.2.1. DIR CLASSIFICATION PROCESS

4.2.1.1. Classification: All DIR ROI or PTV region?

Firstly, the rCT had to be approved for dose calculation. This also meant it was a successful case of DIR. On the first ten patients analysed, we had a total of 36 CBCT scans: 3 of the patients were submitted to 5 SBRT fractions and 7 of the patients were submitted to 3 SBRT fractions. The qualitative classification was made considering all the ROI of DIR, and then changed by considering the PTV region (Figure 3.2). The latter by suggestion of the radiation oncologist, since the delivered dose on PTV and CTV would be analysed further in this dissertation.

It was performed CD and SGD registration to acquire two rCT correspondent to each CBCT scan available (CD and SGD rCT's). The rCT's were compared with the correspondent CBCT and were classified qualitatively according to Table 3.1.

Table 4.3: Comparison between the classification considering only the PTV region and considering all the ROI of registration. Qualitative classification of the CBCT Corrected Deformable (CD) rCT's from the first ten patients. 36 rCT's in total.

		PTV						
		I	II	III	IV	V	VI	VII
ROI	I	0	0	0	0	0	0	0
	II	0	2	1	2	0	0	0
	III	0	0	2	3	2	2	0
	IV	0	1	0	1	6	3	0
	V	0	0	0	0	2	2	1
	VI	0	0	0	1	0	1	1
	VII	0	0	0	0	0	2	1

From Table 4.3, it is possible to calculate, that 25.0% of the created CD rCT's had the same classification whether considering only the PTV region, whether the whole ROI for deformation. However, 63.9% of the rCT's had better classification when considering the PTV region, and only 11.1% had better classification when considering the whole ROI.

Table 4.4: Comparison between the classification considering only the PTV region and considering all the ROI of registration. Qualitative classification of the structure guided deformable (SGD) rCT's from the first ten patients. 36 rCT's in total.

		PTV						
		I	II	III	IV	V	VI	VII
ROI	I	0	0	0	0	0	0	0
	II	0	0	0	2	1	1	0
	III	0	0	0	0	0	1	0
	IV	0	0	0	0	2	5	2
	V	0	0	0	0	3	9	0
	VI	0	0	0	0	0	0	5
	VII	0	0	0	0	0	3	2

As it is notable also on Table 4.4, the rCT's had again usually better classification when considering exclusively the PTV region for classification, now using SGD registration. As it is notable, 13.9% of the SGD rCT's had the same classification on both methods of classification, 77.8% had better classification when considering only the PTV region, and only 8.3% had better classification when considering the whole ROI.

It is crucial that the rCT's have a good result in the PTV region, since PTV region includes the surrounded area actually irradiated in RT treatments. It is critical that the PTV, and subsequently the CTV, receive the prescribed dose.

Since one of the objectives is to perform CT-CBCT DIR to evaluate the actual delivered dose to the clinical study patients, it is it is reasonable to consider only the PTV region for classification of the rCT's. Also, it is visible that there are better classification results when considering only this region.

4.2.1.2. Classification: differences between CD and SGD rCT's

On this phase, the aim was to identify which of both applied DIR methods was the most adequate to use in gynaecological scans of the study cases.

In total, were used 23 patients were analysed: 8 were submitted to 5 fractions of treatment and 15 were submitted to 3 fractions of treatment. This resumed in a total of 85 CBCT's. For every CBCT, after performing CBCT-pCT registration, were created two rCT's, one resultant from CD DIR and other resultant from SGD DIR.

From all the created rCT's (85 CD and 85 SGD) 37.6% of CD rCT's and 74.1% of SGD rCT's were considered approved, which indicates that SGD may have significantly better results that CD. The following tables show the percentage of rCT's which belonged to each classification category[h]:

Table 4.5: Percentage of CD rCT's that belong to each classification category.

	[CD rCT] Classification category						
	I	II	III	IV	V	VI	VII
	Non-approved					Approved	
Relative frequency	0.0%	9.4%	9.4%	18.8%	24.7%	29.4%	8.2%
	62.4%					37.6%	

Table 4.6: Percentage of SGD rCT's that belong to each classification category.

	[SGD rCT] Classification category						
	I	II	III	IV	V	VI	VII
	Non-approved					Approved	
Relative frequency	0.0%	0.0%	0.0%	5.9%	20.0%	48.2%	25.9%
	25.9%					74.1%	

On Figure 4.13 and Figure 4.14 it is possible to visualise the relative frequency of qualitative classifications of each analysed structure of CD and SGD rCT's. On CD and SGD rCT's, the balloon is the structure that has the highest percentage of well succeeded cases, probably due to its clear margins. The structures were generally better classified when in SGD rCT's. The cylinder, on both type of rCT's, proves to be the most difficult structure to deform: the percentage of well classified reshaped cylinders, even though higher in SGD rCT's, is lower than 50% in both SGD and CD rCT's. This may be related to the fact that the insertion of cylinder may not be consistent during treatment, and there is a difficulty in cylinder insertion, associated with previous EBRT treatments.

[h] Classification of the rCT's according to Table 3.1

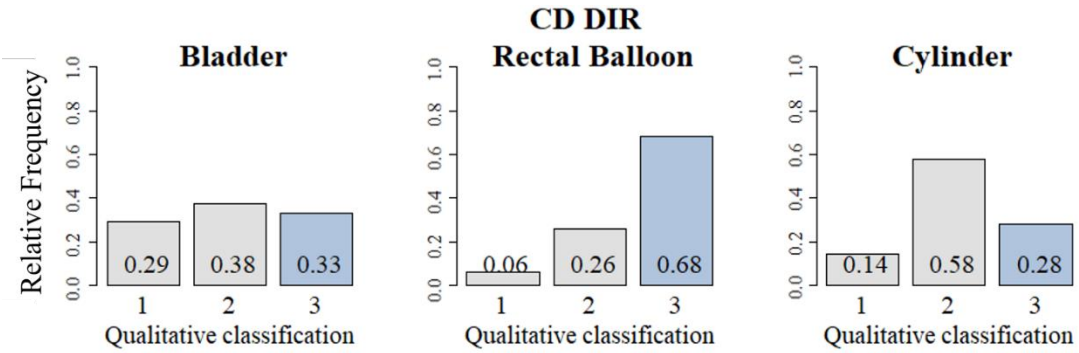

Figure 4.13: Qualitative classification of **CD rCT's** structures.

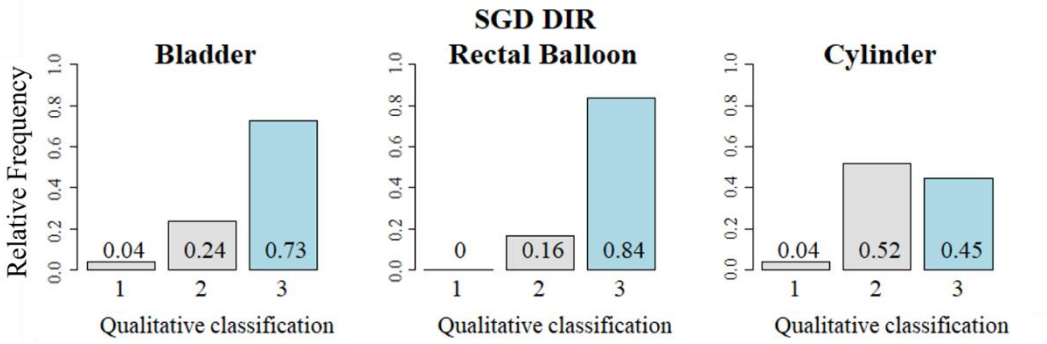

Figure 4.14: Qualitative classification of **SGD rCT's** structures.

The classification of the equivalent pairs of rCT's (SGD and CD) was then compared, and Figure 4.15 sums the results.

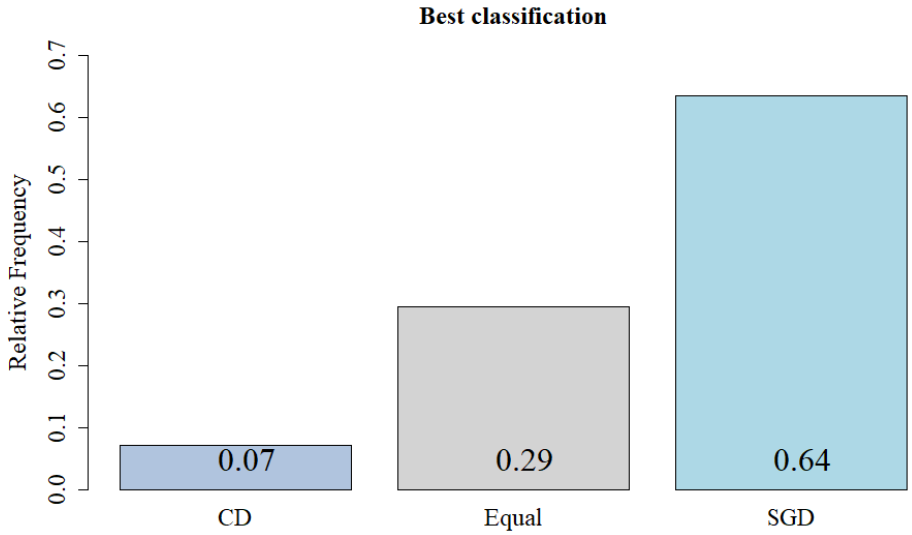

Figure 4.15: Histogram: rCT's better classified with CD, with SGD and equally classified.

As it is possible to visualise, 64% of the created rCT's were better classified when using SGD DIR, 7% were better classified when using CD DIR and 29% had the same classification.

As stated before, Velocity® user manual suggests that SGD DIR is adequate when CD deformation does not achieve satisfactory results. The results suggest that SGD can improve significantly the results of a rCT created using CD registration.

From the acquired data, and since there is still 7% of the rCT's that were better when using CD DIR, it was decided not to choose *a priori* one of the methods to perform DIR to gynaecological scans.

The influence of the DIR method not only on deformation area, but also considering each organ separately was studied. Figure 4.16 shows the percentage of best classified organs achieved by comparing the analogous organs on the paired rCT's created.

.

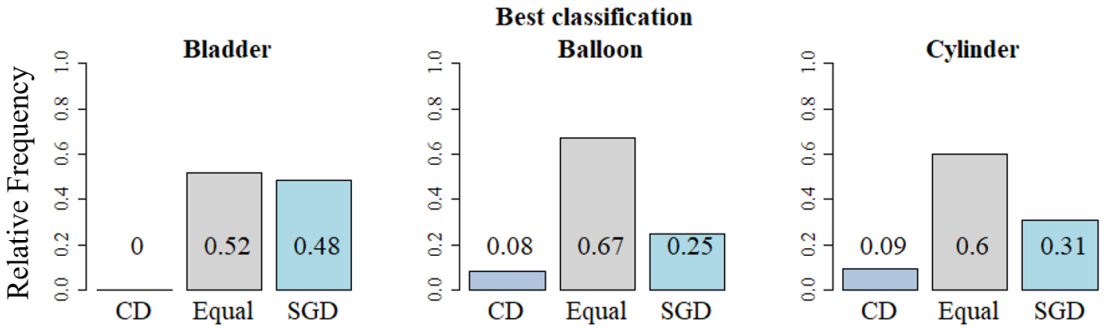

Figure 4.16: Best classified rCT's - by organ.

When analysing the rCT's bladder, 52% of the reshaped bladders had the same classification on both acquired rCT's. However, 48% had better classification in SGD rCT's.

When analysing the balloon deformation, 67% had equal classification in both rCT's acquired. 8% had better classification in CD rCT's and 25% had better classification in SGD rCT's.

60% of the reshaped cylinders were equally classified in both rCT's. 31% were better classified in the SGD rCT's and 9% were better classified in the CD rCT's.

This data enhances the impression that even though there is always a percentage higher than 20% of the created SGD rCT's that results in better classified organs, there is a considerate percentage of structures that is equally classified in both analogous rCT's.

This data indicates that we need to consider both the alternative methods. Therefore, since CD is a simpler and less time-consuming method, it is reasonable to perform firstly SGD DIR to assure the same DIR ROI if needed. Then, if the results are not enough satisfactory, try CD.

It was also tested the differences in $m_{conformality}$ [(Equation (3.2)] between the two acquired rCT's. On Figure 4.17, it is possible to visualise that the median of mean conformality value of CD and SGD rCT's is apparently higher in $m_{conformality}$ of SGD rCT's.

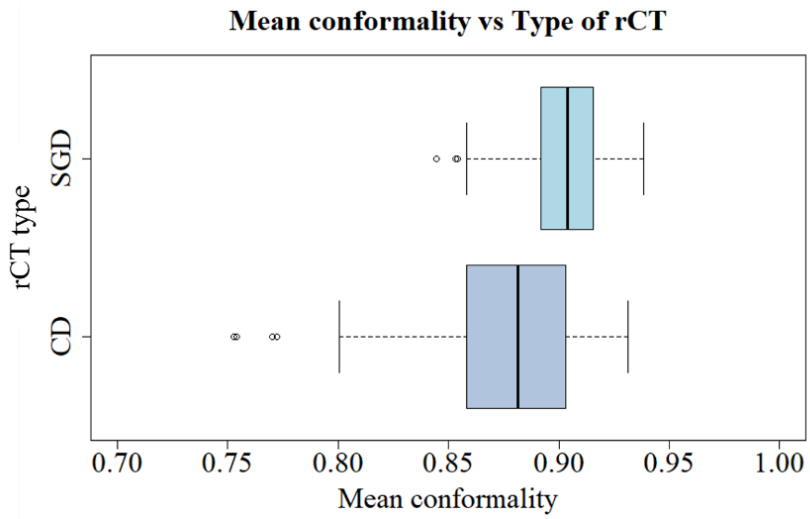

Figure 4.17: Mean conformality of CD and SGD rCT's.

The differences of the two samples (N = 85) were tested using the non-parametric Wilcoxon test, since both related samples were proved not to be normal. Wilcoxon test showed that the $m_{conformality}$ median of SGD rCT's is significantly higher than $m_{conformality}$ of CD rCT's ($W = 3529, p \ll \alpha, \alpha = 0.01$) enhancing that SGD has better results than CD [67].

4.2.1.3. Classification: conformality vs qualitative classification

Measuring the conformality between the reshaped structure (resultant from the propagation of CBCT contours) and the one contoured on the CBCT, might be a possible way to measure the rCT's quality.

It was calculated the $m_{conformality}$ of the three structures, as explained in Equation (3.2) in all the acquired rCT's and the next objective was to find the correlation between the $m_{conformality}$ and the qualitative classification of the rCT's, building first the boxplots presented in Figure 4.18.

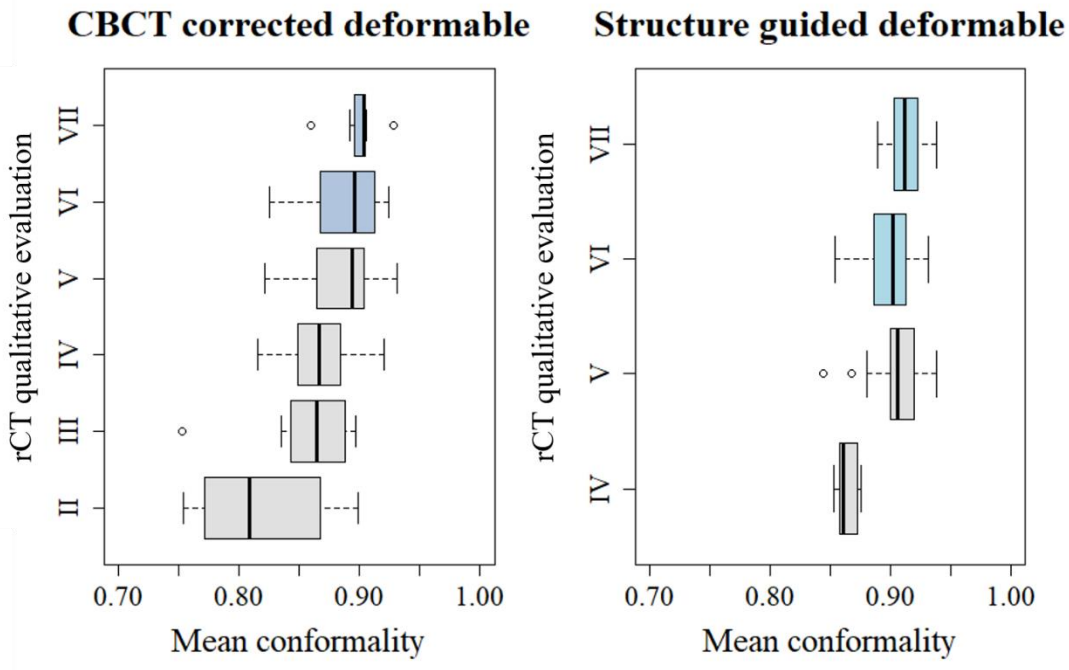

Figure 4.18: Boxplots: mean conformality vs rCT's qualitative evaluation [CD rCT's on left and SGD rCT's on right]. No CD rCT's included in classification category I. No SGD rCT's included in classification categories I, II and III.

In Figure 4.18, it seems that $m_{conformality}$ is correlated with the qualitative evaluation on CD rCT's, contrary to SGD rCT's. It is visible on the left boxplot that the mean conformality median of better classified CD rCT's is positioned at higher values. Nevertheless, the boxplots are not enough to explain a correlation, and it is needed to proof this correlation by performing binomial logistic regression (for CD and SGD), and considering as the independent variable the $m_{conformality}$ value and as the dependent variable the approval of the rCT (0 – not approved or 1 - approved) [68], [69].

First, it was proven the approximated logit linearity for CD rCT $m_{conformality}$ values. At this phase, it was proven that there was no logit linearity for SGD rCT $m_{conformality}$, and that is also visible on Figure 4.18 and Figure 4.19 where it seems that the values of SGD rCT's $m_{confomality}$ do not increase linearly when the rCT's are higher classified [68], [69].

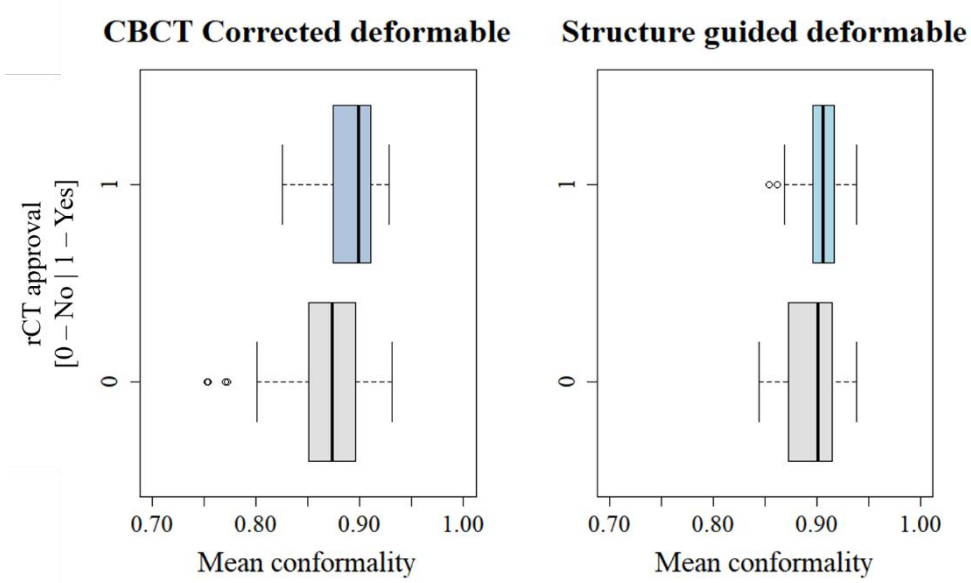

Figure 4.19: Boxplot: Approved rCT's vs Conformality [CBCT corrected deformable on left and structure guided deformable at right]

Considering that a rCT is approved only if its qualitative classification is VI or VII, the rCT's were divided into two groups, approved (1) and non-approved (0), and then were compared with $m_{conformality}$ median values. The acquired data was visualised in the boxplots of Figure 4.19.

On Figure 4.19, it seems that the $m_{Conformality}$ median of approved CD rCT's is positioned in a higher value in the first boxplot. However, the $m_{Conformality}$ median of approved and non-approved SGD rCT's is similar.

To compare the $m_{Conformality}$ values of both non-related samples (approved and non-approved rCT's) it was performed the non-parametric Mann-Whitney test [67], since the samples were proved not to be normal. This test compared the median of approved rCT's (M_1) with the median of non-approved rCT's (M_0):

$$H_0: M_1 \leq M_0$$
$$H_1: M_1 > M_0 \quad (4.1)$$

The test was made twice, one for CD rCT's, and one for SGD rCT's.

The tests showed that the median of $m_{Conformality}$ of approved CD rCT's was significantly higher than median of $m_{Conformality}$ of non-approved rCT's. It was also proven that the $m_{Conformality}$ median of approved

SGD rCT's is not significantly higher from the median of non-approved SGD rCT's. The resume of both tests is presented on Table 4.7 [67].

Table 4.7: Mann-Whitney tests results. Comparison between approved and non-approved CD and SGD rCT's $m_{conformality}$ median.

rCT's	N	α	p	W
CD	85	0.01	0.0018	1192
SGD			0.1635	832

The SGD method is based not only on intensity of pixels, but also on the correspondent contours of the moving and fixed image. Therefore, it was expected that $m_{conformality}$ of it resultant rCT's is higher and cannot be a predictor of a successful DIR case. Therefore, it was not justified to find a model to predict SGD rCT's approval depending on $m_{conformality}$ value.

Nevertheless, it was created logistic binomial regression, to find the probability of a CD rCT being approved depending on the $m_{Conformality}$ value of the correspondent rCT, which had the following structure [68], [69]:

$$\log \frac{P_{app[CD]}}{1 - p_{app[CD]}} = \beta_0 + \beta_1 \times m_{conformality} \quad (4.2)$$

From Equation (4.2), $P_{app[CD]}$ is the probability of a CD rCT being considered approved according to the created model, β_0 corresponds to the expected value for the logarithm of the chance of rCT approval when $m_{conformality} = 0$ and β_1 corresponds to the expected variation in the value for the logarithm of the chance of a CD rCT being considered approve due to the increment in $m_{conformality}$. From the created model using R Studio, $\beta_0 = -3.295$ and $\beta_1 = 4.185$ [68], [69].

$$P_{app[CD]} = \frac{e^{\beta_0 + \beta_1 \times m_{conformality}}}{1 + e^{\beta_0 + \beta_1 \times m_{conformality}}} \quad (4.3)$$

This created model [Equations (4.2) and (4.3)] was then tested using the Chi-squared adjusted test, and it was confirmed that the probability of a CD rCT being considered approved ($P_{app[CD]}$ for CD) is significantly correlated with a higher value of $m_{conformality}$ ($N=85, \chi^2_{obs}=11.02$, $p \ll \alpha$, $\alpha=0.01$).

If considered that when the $P_{app[CD]} \geq 0.6$, a CD rCT was considered approved, the confusion matrix resultant from the previous model is [68], [69]:

Table 4.8: Confusion Matrix. Binomial regression model: CD rCT approval depending on $m_{conformality}$ value

	Non-approved rCT's	Approved rCT's
$P_{app[CD]} \geq 0.6$	20 False Negative (FN)	22 True Positive (TP)
$P_{app[CD]} < 0.6$	33 True Negative (TN)	10 False Positive (FP)

According to Table 4.8 , there were 30 poorly classified rCT's and 55 well classified rCT's resultant from the model. Subsequently, the model's Positive (PPV) and Negative (NPV) predictive values are the following:

$$\mathrm{PPV} = \frac{\mathrm{TP}}{\mathrm{TP} + \mathrm{FN}} = 0.52 \tag{4.4}$$

$$\mathrm{NPV} = \frac{\mathrm{TN}}{\mathrm{TN} + \mathrm{FP}} = 0.77 \tag{4.5}$$

These results [(4.4) and (4.5)] indicate than when considered approved a CD rCT after , there is 52% of chances approving a CD rCT it is actually considered approved and 77% of chances of suggestion of not approving a CD rCT when it is non-approved.

The fact that in this model, the probability of an rCT being approved when the $m_{conformality}$ equals 1 is different than 1, enhances the fact that it is not possible to use the $m_{conformality}$ the only tool to approve a CD rCT.

Afterwards, and now not considering the previous model, it was aimed to find the inflection point of $m_{conformality}$ value to consider when approving a CD rCT: now by considering the sample rCT's approved if its $m_{conformality}$ values were above different inflection points (x). The qualitatively approved and non-approved rCT's were compared with the approved and non-approved rCT's with this method. It was then, possible to calculate the percentage of false approved and non-approved rCT's when considering different inflection points. The following table explains the method:

Table 4.9: False positives (FP), false negatives (FN), true positives (TP) and true negatives (TN), associated to a fixed $m_{conformality}$ inflection point (x)

	$m_{conformality}$	
	$< x$ Non-approved rCT's	$\geq x$ Approved rCT's
0 Non-approved rCT's	TN	FP
1 Approved rCT's	FN	TP

In order to find the inflection point to differentiate approved from non-approved CD rCT's, were fixed 16 $m_{conformality}$ values (x from Table 4.9), and for the CD rCT's we found the percentage of false approved (FP) and false non-approved (FN) rCT's resultant. The results are available on Table 4.10.

Table 4.10: Percentage of false negatives and false positively classified rCT's when considering different inflection points (x) of mean conformality

x	%FN+%FP
0.80	58
0.81	56
0.82	54
0.83	54
0.84	51
0.85	51
0.86	47
0.87	41
0.88	38
0.89	35
0.90	**28**
0.91	34
0.92	34
0.93	39
0.94	38
0.95	38

By analysing Table 4.10, when considering the data of CD rCT's, it is possible to visualise that the lowest percentage of false positives plus false negatives is when it is considered the inflection point of $m_{conformality}$ fixed at 0.90. This value indicates that theoretically, $m_{coformality}$ is above 0.9, there is an higher probability of this CD rCT being considered approved.

However, this data does not allow the approval of an rCT based only on the mean conformality value.

As it was confirmed in this chapter, conformality is a tool that may help to indicate a success or non-success of the DIR intensity-based process, using CBCT corrected deformable on Velocity®. Nevertheless, it is not possible to approve a rCT using only this tool, since it is not accurate enough as it was shown by the probability functions created.

4.2.1.4. Classification: patients with or without uterus

This chapter is focused in studying the differences in rCT's quality of patients with or without uterus (5-fraction and 3-fraction SBRT treatment, respectively), due to the differences referenced in chapter 3.3.2. Were acquired 40 CD rCT's 40 SGD rCT's from the patients with uterus and 45 CD rCT's and 45 SGD rCT's from the patients without uterus.

When comparing CD rCT's of patients with and without uterus it is notable that there is a higher percentage of approved rCT's of patients whose uterus was surgically removed. As it is possible to visualise in Table 4.11 and Table 4.12, there is a considerable higher percentage of rCT's in the VI and VII classification categories (58.0%) when speaking of patients without uterus, than in patients with uterus (15.0%). As in the CD rCT's, the higher relative frequency of well classified SGD rCT's is on the 3fr patient cases. There were 80.0% of approved 3fr SGD rCT's versus 68.0% of approved 5fr SGD rCT's (Table 4.13 and Table 4.14)

Table 4.11: Percentage of rCT's that belong to each qualitative category. CD rCT's of patients without uterus.

	Category [CD rCT – Without uterus]						
	I	II	III	IV	V	VI	VII
	Non-approved					Approved	
Relative frequency (%)	0.0%	4.4%	8.8%	13.3%	15.6%	46.6%	11.1%
	42.0%					58.0%	

Table 4.12: Percentage of rCT's that belong to each qualitative category. CD rCT's of patients with uterus.

	Category [CD rCT – With uterus]						
	I	II	III	IV	V	VI	VII
	Non-approved					Approved	
Relative frequency (%)	0.0%	15.0%	10.0%	25.0%	35.0%	10.0%	2.0%
	85.0%					15.0%	

Table 4.13: Percentage of rCT's that belong to each qualitative category. SGD rCT's of patients without uterus.

	Category [SGD rCT – Without uterus]						
	I	II	III	IV	V	VI	VII
	Non-approved					Approved	
Relative frequency (%)	0.0%	0.0%	0.0%	6.7%	13.3%	46.7%	33.3%
	20.0%					80.0%	

Table 4.14: Percentage of rCT's that belong to each qualitative category. SGD rCT's of patients with uterus.

	Category [SGD rCT – With uterus]						
	I	II	III	IV	V	VI	VII
	Non-approved					Approved	
Relative frequency (%)	0.0%	0.0%	0.0%	5.0%	27.5%	50.0%	17.5%
	32%					68.0%	

After, were compared the qualitative classifications of the contoured structures, of 3fr and 5fr patients of CD and SGD rCT's (Figure 4.20, Figure 4.21, Figure 4.22 and Figure 4.23). Once again, SGD rCT structures are usually better classified than CD rCT structures.

It is noticeable by the plots, that on CD rCT's of patients without uterus (Figure 4.20), the percentage of well classified reshaped structures is always higher than in patients with uterus (Figure 4.21).

From Figure 4.22 and Figure 4.23, it is clear that the relative frequency of the well classified structures (qualitative classification equals 3) is not considerably different in the SGD rCT's, probably since this is a method that is not exclusively intensity-based. However, there is a higher percentage of well classified reshaped bladders and cylinders on the SGD rCT's on 3fr patients.

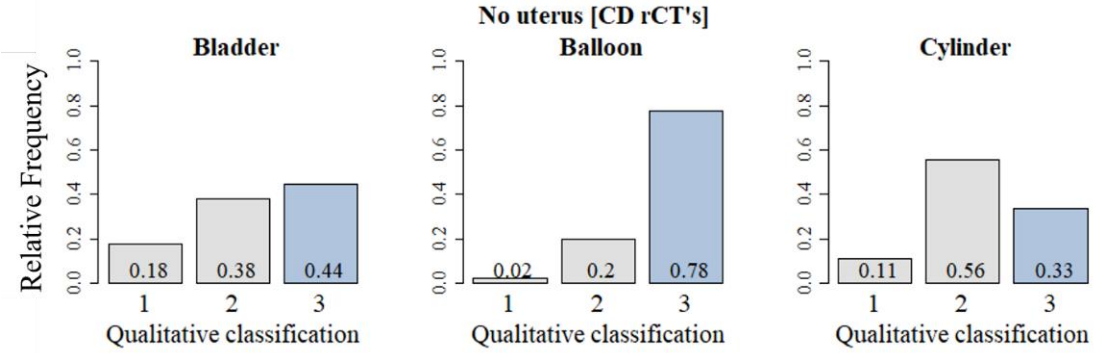

Figure 4.20: Relative frequency of qualitative classifications by structure. Patients whose **uterus was surgically removed CD rCT's.**

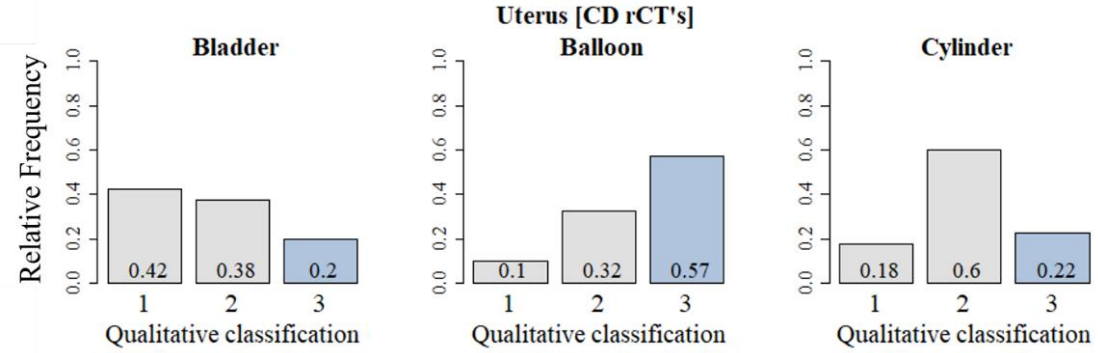

Figure 4.21: Relative frequency of qualitative classifications by structure. Patients whose **uterus was not surgically removed CD rCT's**.

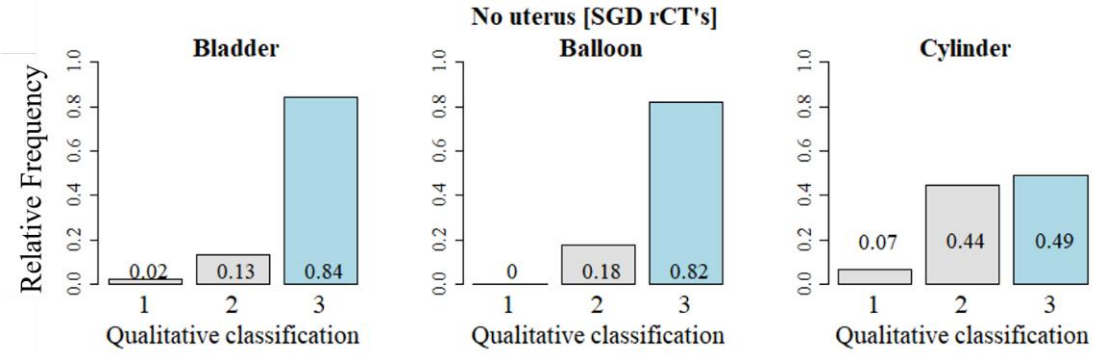

Figure 4.22: Relative frequency of qualitative classifications by structure. Patients whose **uterus was surgically removed SGD rCT's**.

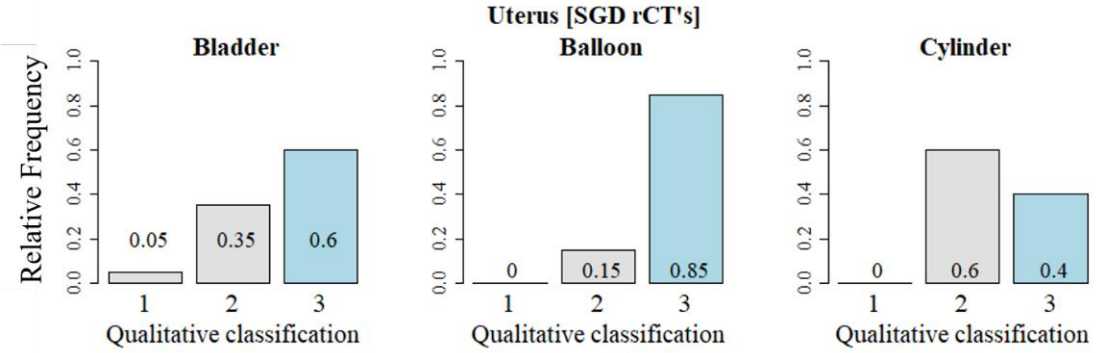

Figure 4.23: Relative frequency of qualitative classifications by structure. Patients whose **uterus was not surgically removed SGD rCT's**.

When analysing the reshaped bladders, it is possible to note that in 3fr patients rCT's (CD and SGD), the percentage of well classified deformed bladders is around 20% higher than in 5fr patients rCT's.

The balloon is apparently the easiest structure to deform, since there is a considerable (minimum 57%) percentage of well classified cases not only on 3fr patients rCT's but also on 5fr patients rCT's, on both CD and SGD rCT's. This can be explained by the marked difference in contrast between the balloon and the surrounding structures, which facilitates the DIR process.

The percentage of well classified reshaped cylinders was always the lowest, and it is lower on 5-fr patient rCT's, which can indicate that this is the most difficult structure to deform, probably due to the difficulty in cylinder insertion before treatment delivery.

4.2.2. DOSE CALCULATION

4.2.2.1. Evaluation of deformation magnitude

When the rCT's were exported to Eclipse®, the delivered treatment was copied to the plan sum of all the patient's exported rCT's. Then the dose map superimposed on the planning CT was calculated (SD as named and described in chapter 3.4).

This first phase allowed the evaluation deformation magnitude of the rCT's, since when analysing the SD on the pCT's we were evaluating the HU differences between the pCT and the plan sum of the rCT's: allowing patients consistency evaluation through treatment.

It was calculated the ratio between the SD and planned dose on both PTV and CTV of all database patients (3fr and 5fr) (Figure 4.24).

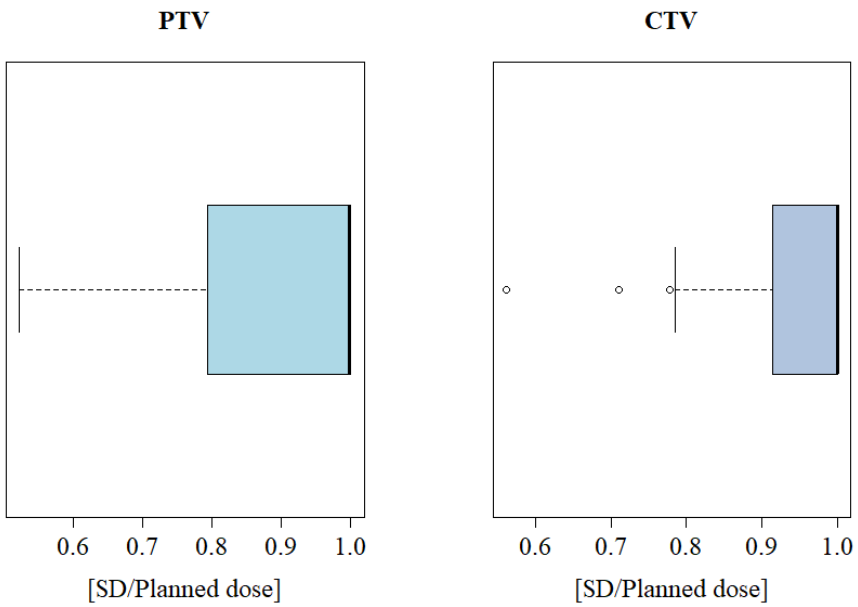

Figure 4.24: Sum dose of all rCT's superimposed over the pCT: ratio of delivered dose / planned dose on PTV (left) and CTV (right).

The mean value of PTV's ratio of SD/planned dose was 87% and the median was 100%. The mean value of CTV's ratio of SD/planned dose was 93% and the median was also 100%. From Figure 4.24, the patients CTV's showed higher consistency through SBRT treatments than the PTV. This is as expected, since the PTV contouring aims the assurance of delivering the prescribed dose to the CTV. The three outliers present in the right boxplot, belong to 5fr SBRT treatment patients.

Since the clinical study SBRT protocol has been being improved through the last three years, it was relevant to study if there were improvements in patient's consistency during treatment along the years (Figure 4.25), since there are studies that suggest that clinical trials have better results in clinics with experience [70].

From Figure 4.25, is clear that through the years, the ratio SD/planned dose has increased, supporting the protocol learning curve. When analysing the PTV, the mean ratio in 2016 was 78%, in 2017 89% and in 2018 96%. On CTV data, the mean ratio of SD/planned dose was 82% in 2016, 94% in 2017 and 100% in 2018.

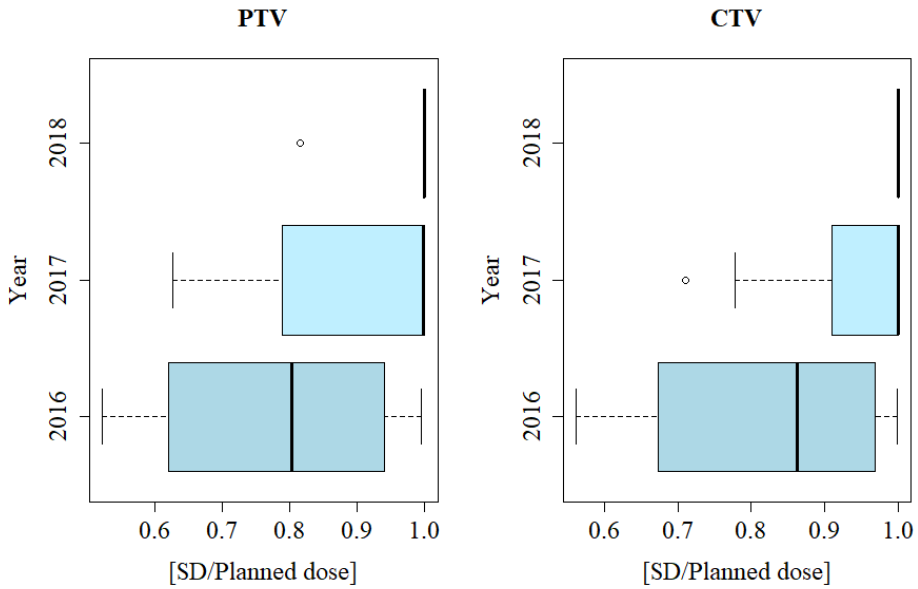

Figure 4.25: Summed dose of all rCT's superimposed over the pCT: ratio of delivered dose / planned dose on PTV (left) and CTV (right) in function of year of treatment of the patient.

When analysing the ratio of SD/planned dose by dividing the patients according to the number of SBRT treatment fractions (Figure 4.26), it was visible that patients with 5fr SBRT treatment (with uterus) had higher differences between the pCT and rCT's. The uterus existence on these patients may result in a higher difficulty of replicating the pCT conditions through treatment. When analysing the ratio on the PTV, the mean ratio of SD/planned dose on 3fr patients was 97% while on 5fr patients was 73%. CTV's mean ratio of SD/planned dose on 3fr patient was 99% and on 5fr patients was 82%.

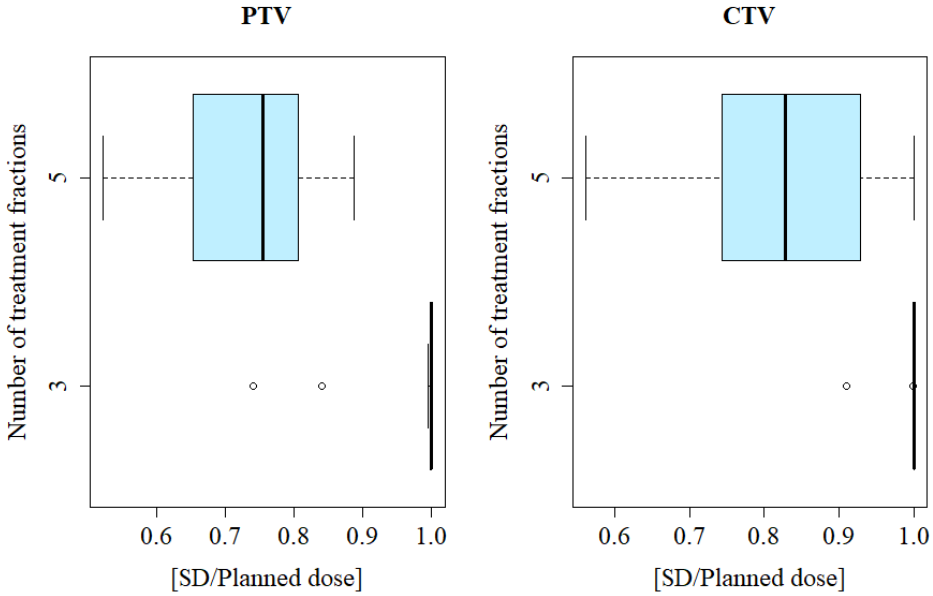

Figure 4.26: Summed dose of all rCT's superimposed over the pCT: ratio of delivered dose / planned dose on PTV (left) and CTV (right) in function of the number of fractions of SBRT treatment.

It is also important to note that we still do not have a high number of patients included in the clinical study and in the DIR requirements previously mentioned: 23 patients (Figure 4.27 represents the number of patients treated in each year). Besides, from these 23 patients, 4 were treated in 2016 and 5 in 2018.

Also, there was only one patient treated with 5fr SBRT in 2018 and only 1 patient treated with 3fr SBRT in 2016. This does not let to conclude if it is the existence of uterus, or the protocol learning curve, that lead to a better consistency of the patients during treatment (which also leads to better DIR results).

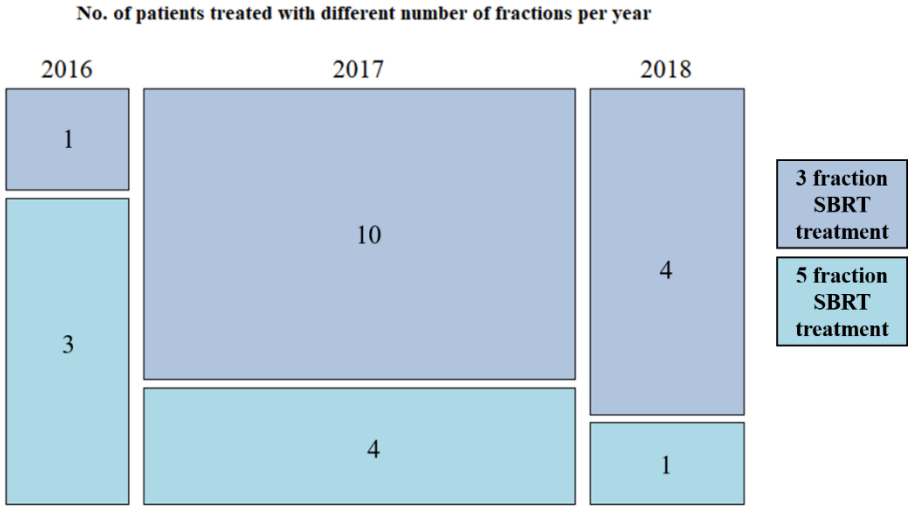

Figure 4.27: Number of patients who passed through the two types of SBRT treatment along the years.

4.2.2.2. Evaluating the actual delivered dose

The calculated doses on Eclipse of each rCT were exported to Velocity®. The deformation matrixes anteriorly created by performing DIR were used to deform the calculated rCT doses to the pCT. After being deformed into the pCT, all fraction doses were summed, and the deformed dose map (Actual delivered dose – ADD) was compared with the planned dose.

It was then calculated the ratio between the ADD and planned dose on PTV and CTV.

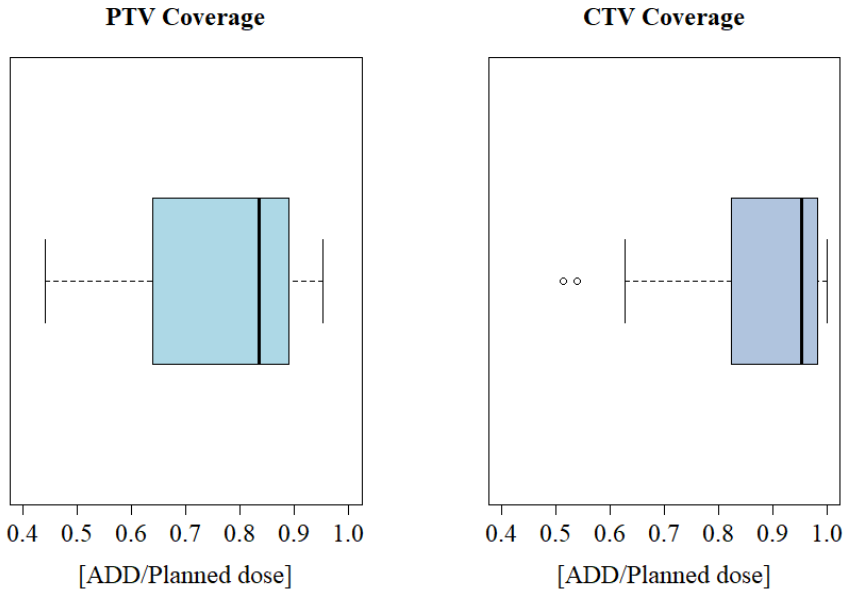

Figure 4.28: Deformed dose maps: ratio of sum of deformed doses and planned dose on PTV (left) and CTV (right) in function of the number of fractions of SBRT treatment.

Figure 4.28 shows the 23 patients PTV and CTV ratio between ADD and planned dose doses distribution.

PTV's median ratio of ADD/planned dose was 83% and the mean was 76%. The CTV's median ratio of ADD/planned dose was 95% and the mean was 88%. This indicates that 50% of all the patients received on the CTV over 95% of the prescribed dose to the PTV. The two outliers present in the right boxplot, belong to 5fr SBRT treatment patients.

When analysing the boxplots of Figure 4.29, it is visible that along the years, the ADD is more approximated to the planned dose as the years increase, on CTV and PTV of all patients.

The mean ratio of ADD/planned dose on the PTV in 2016 was 67%, in 2017 was 77% and in 2018 was 83%. The mean ratio of ADD/planned dose on CTV was slightly higher: in 2016 was 77%, in 2017 was 89% and in 2018 was 94%. The outlier comes from a 5fr SBRT patient.

Another possible reason is that in 2018 and in 2017 there was a predominance of 3fr SBRT treatment patients, and the existence of uterus in a patient might be correlated with the delivery of the planned dose.

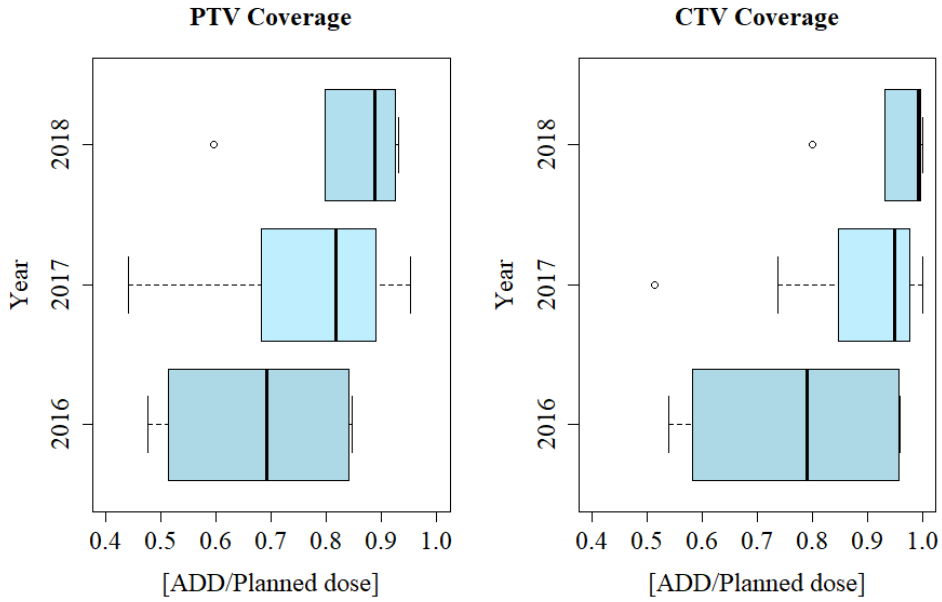

Figure 4.29: Deformed dose maps: ratio of sum of deformed doses and planned dose on (left) and CTV (right) in function of year of treatment of the patient.

On Figure 4.30 it was analysed the ratio of ADD/planned dose on CTV and PTV, depending on the type of patient. 3fr patients were patients whose uterus had been surgically removed, with a smaller PTV, and 5fr patients were patients with uterus, and subsequently with a larger PTV.

It is visible on Figure 4.30 boxplots, that in 5fr-patients the ratio ADD/planned dose was apparently lower (on CTV and PTV) than in 3fr patients.

For 5fr patients, the mean value of ratio ADD/planned dose on PTV was 59% and on CTV was 72%. For 3fr patients, the mean value of ratio ADD/planned dose on PTV was 86% and on CTV was 97%.

3fr patients seem to be receiving a higher percentage of the planned dose than 5fr patients, and this may be related to the fact that is difficult to replicate the protocol of the clinical study through more sessions of treatment, and with patients whom uterus has not been surgically removed.

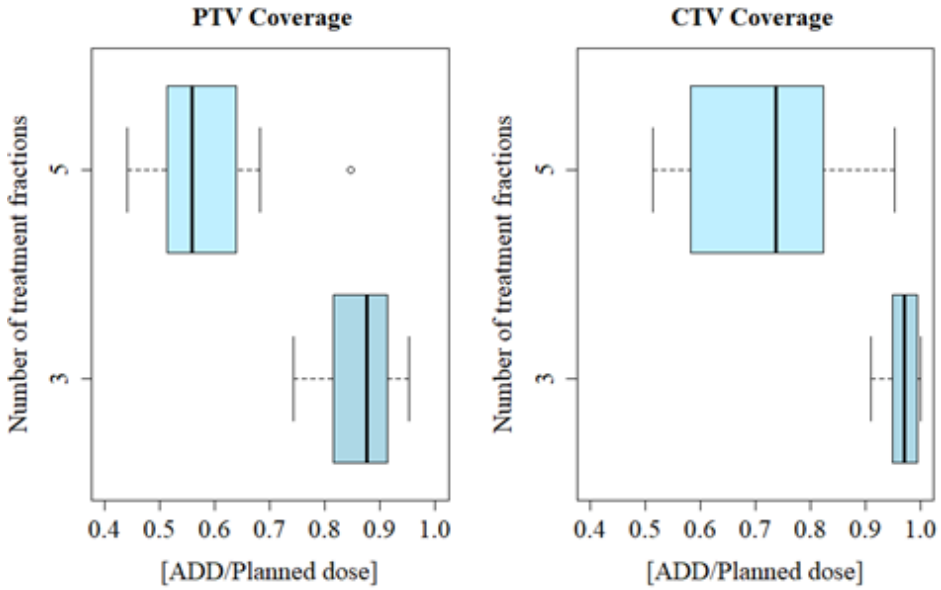

Figure 4.30: Deformed dose maps: ratio of sum of deformed doses and planned dose on PTV (left) and CTV (right) in function of the number of fractions of SBRT treatment.

The delivered doses to the following organs at risk were also analysed: small bowel, rectal wall and bladder wall. It was checked if these structures received a higher dose value than the limit established by the radiation oncologist at each prescribed treatment.

In some patients, it was not possible to measure the values of received dose to some of these structures. This was due either because the radiation oncologist did not prescribe a maximum dose value, or because the structure was not contoured by the radiation oncologist. The fact that not all the structures are contoured is because they lay out from the target.

It was calculated the value of relative difference between the actual delivered dose and the maximum allowed dose (prescribed by the radiation oncologist) [Equation (4.6)] on small bowel, rectal wall and bladder wall for each patient, and the data is available in Figure 4.31.

$$\text{Relative difference} = \frac{\text{Actual delivered dose}}{\text{Maximum allowed dose}} - 1 \qquad (4.6)$$

Figure 4.31 shows that small bowel was the structure that had the highest number of patients who received higher dose than planned: in the first graphic, there are 7 out of 15 patients received higher dose values than the maximum allowed by the radiation oncologist. However, all of these patients received less dose than de allowed in clinical practice, which is based on dose limits established in 2008 [71].

Only 2 out of 22 and 1 out of 23 patients, received, a higher dose value than the allowed on the rectal and bladder wall, respectively. Also, these were cases where the clinical practice dose limits were respected.

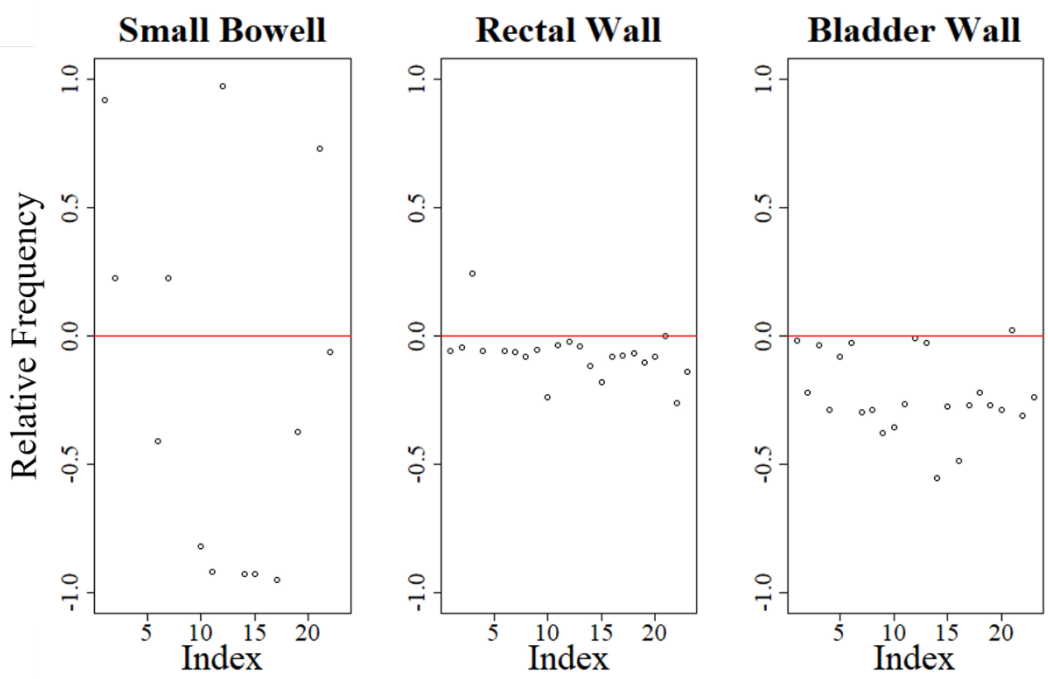

Figure 4.31: Relative difference between actual delivered dose and maximum dose allowed on small bowel, rectal wall and bladder wall. Dots above the red line: patients' fraction of dose outside the limit of allowed dose.

5. CONCLUSION

Velocity's applicability on clinic

As suggested by the radiation oncologist, the approval of an rCT was based only by evaluating the deformation on the PTV region, since the final objective was to analyse the delivered dose on PTV and correspondent CTV.

SGD DIR was a method that, as expected, resulted in better rCT's than CD: 74.1% of the SGD rCT's were considered approved while only 37.6% of the CD rCT's were considered approved. Besides, when comparing the all the pairs of rCT's correspondent to the same CBCT (CD and SGD), 64% were better classified when using SGD DIR. The median of SGD rCT's $m_{conformality}$ was proven to be statistically higher than CD rCT's $m_{conformality}$, probably because SGD uses a hybrid objective function (chapter 2.1.2.1).

Nevertheless, when analysing the classification of the same structures on correspondent rCT's, it indicated that there was a high percentage of equally classified structures on both rCT's than in one method specifically.

The acquired data also shown in chapter 4.2.1.2, indicates that on these study patients, the cylinder is usually the most difficult structure to deform, since it is the structure with the lowest percentage of well classified structures. This may be related to the fact that the insertion of cylinder may not be consistent during treatment.

When analysing the potentiality of using $m_{conformality}$ as a way of approving a rCT, it was proven that $m_{conformality}$ is correlated only with the qualitative classification of CD rCT's. This may be due to the priority in achieving the best conformality possible between the pCT and CBCT contours in SGD DIR. The results also suggested that when considering the created model, if considered approved a CD rCT with $P_{app[CD]}$ above 0.6, there were 52% and 77% of chances of a CD rCT being correctly considered approved or non-approved, respectively. Also, from the sample, $m_{conformality}$ fixed at 0.90 seemed to be an adequate inflection point, to consider a CD rCT approved. Nevertheless, it is important to emphasize that it is always necessary the qualitative evaluation of the CD rCT's, despite of the created classification helping tools.

Due to the acquired data, we concluded that it is indicated to these patients, to firstly perform SGD DIR, and if the results are not good enough, try to use CD DIR. When classifying a CD rCT, the $m_{conformality}$ can be a tool which helps in the rCT qualitative classification described.

By evaluating the values of SD/planned dose, it is possible to infer that through the last three years, the uniformity of patients (which is correlated with the protocol learning curve) has improved. However, the low number of patients (23) does not let to conclude if it is due to the protocol rigor or type of patient that guarantees a better uniformity during treatment.

Through the last three years, the actual delivered dose (ADD) has been approximating the planned dose, which can also be related also with the protocol learning curve. Nevertheless, since the number of 3fr patients is higher than 5fr patients in 2017 and 2018, it may indicate that the actual delivered dose can also be correlated with the type of patient, indicating that 5fr patients seem to be receiving less percentage of the planned dose than 3fr patients.

However, it is not possible to affirm that 5fr patients are not receiving enough dose in the PTV and CTV. Firstly, in brachytherapy, it was not yet been evaluated the actual delivered dose that reaches the PTV, so we cannot affirm that these patients are not receiving enough dose as they would receive in brachytherapy since we still do not have data for comparison purposes. Secondly, these patients have been showing good reply to SBRT, which mainly aims to avoid tumour recurrence.

The actual delivered dose to organs at risk, despite being sometimes out of the limits imposed by the radiation oncologist, was always inside clinical practice tabled limits. This showed how rigorous the protocol is, and that the OAR's were not put at risk.

As seen, DIR can be used successfully when the objective is to deform abdominal-pelvic CT scans into the form of CBCT scans and showed good results to be used on clinic. Velocity® is simple and user-friendly software.

Velocity® can be used to make sure if patients who pass through SBRT (which implies the prescription of high dose) are receiving the planned dose. If the planned conditions are not achieved, it is possible if using Velocity®, to adapt the treatment. Also, it can be used when in doubt of re-planning.

Future work

There are still Velocity® tools which were not explored in this project and can be used on clinic such as automated contouring.

It would be interesting to study DIR in other cancer cases, and to explore if Velocity® can be successful performing DIR in other type of scans.

For future implementation of Adaptative Radiation Therapy on clinical daily practice, Velocity may be an adequate software to perform this using DIR.

About the delivered dose of our study cases, it will be needed more patients, and more follow up years, to conclude if this treatment is achieving better results than brachytherapy as it has been suggesting.

6. REFERENCES

[1] W. Hahn and R. Weinberg, "Rules for making human tumour cells," *Nejm*, vol. 347, no. 20, pp. 1593–1604, 2002.

[2] "What Are Tumors?" [Online]. Available: http://pathology.jhu.edu/pc/BasicTypes1.php?area=ba. [Accessed: 13-Oct-2017].

[3] "How is cancer diagnosed?" [Online]. Available: https://www.cancer.org/treatment/understanding-your-diagnosis/tests/testing-biopsy-and-cytology-specimens-for-cancer/how-is-cancer-diagnosed.html. [Accessed: 13-Oct-2017].

[4] "Treatment for Cancer - National Cancer Institute." [Online]. Available: https://www.cancer.gov/about-cancer/treatment. [Accessed: 13-Oct-2017].

[5] A. Urruticoechea, R. Alemany, J. Balart, A. Villanueva, F. Viñals, and G. Capellá, "Recent Advances in Cancer Therapy: An Overview," *Curr. Pharm. Des.*, vol. 16, pp. 3–10, 2010.

[6] "Chemotherapy." [Online]. Available: https://www.ncbi.nlm.nih.gov/pubmedhealth/PMHT0024232/. [Accessed: 16-Oct-2017].

[7] "How does chemotherapy work?," 14-Jan-2016. [Online]. Available: https://www.ncbi.nlm.nih.gov/pubmedhealth/PMH0072611/. [Accessed: 16-Oct-2017].

[8] J. Cleary, H. Gelband, and J. Wagner, *Cancer: Disease Control Priorities*. 2015.

[9] E. B. Podgorsak, *Radiation Oncology Physics: A Handbook for Teachers and Students*, vol. 98, no. 5. 2008.

[10] H. E. Johns and J. R. Cunningham, *Physics of Radiation Therapy*, vol. 467. 2001.

[11] "External Beam Radiation Therapy." [Online]. Available: https://www.cancer.org/treatment/treatments-and-side-effects/treatment-types/radiation/external-beam-radiation-therapy.html. [Accessed: 06-Nov-2017].

[12] "How radiation affects cells." [Online]. Available: http://www.rerf.jp/radefx/basickno_e/radcell.htm. [Accessed: 17-Oct-2017].

[13] "Intracavitary Radiation Treatments for cancer of the cervix." [Online]. Available: http://www.aboutcancer.com/intracavitary_radiation_treatments.htm. [Accessed: 14-Dec-2017].

[14] R. Banerjee and M. Kamrava, "Brachytherapy in the treatment of cervical cancer: A review," *Int. J. Womens. Health*, vol. 6, no. 1, pp. 555–564, 2014.

[15] Sociedade Portuguesa de Ginecologia, "Cancro ginecológico - Consensos nacionais 2016," 2016. [Online]. Available: http://www.spginecologia.pt/consensos/cancro-ginecologico-consensos-nacionais-2016.html. [Accessed: 29-Nov-2018].

[16] O. Journals, "ICRU Report 83 - Prescribing, Recording, and Reporting Photon-Beam Intensity-Modulated Radiation Therapy."

[17] N. Smith and A. Webb, *Introduction to medical imaging: physics, engineering, and clinical applications*. 2011.

[18] R. Rai *et al.*, "The integration of MRI in radiation therapy : collaboration of radiographers and radiation therapists," pp. 61–68, 2017.

[19] M. A. Schmidt and G. S. Payne, "Europe PMC Funders Group Radiotherapy Planning using MRI," vol. 60, no. 22, pp. 1–50, 2016.

[20] "SPECT vs PET." [Online]. Available: https://radiopaedia.org/articles/spect-vs-pet. [Accessed: 18-Oct-2017].

[21] M. N. Wernick and J. N. Aarsvold, *Emission Tomography: the Fundamentals of PET and SPECT*, vol. 23, no. 4. 2005.

[22] "Nuclear Medicine | National Institute of Biomedical Imaging and Bioengineering." [Online]. Available: https://www.nibib.nih.gov/science-education/science-topics/nuclear-medicine. [Accessed: 18-Oct-2017].

[23] J. T. Bushberg, J. A. Seibert, E. M. Leidholdt Jr., and J. M. Boone, *The Essential Physics of Medical Imaging (2nd Edition)*. 2002.

[24] G. Omami, D. Tamimi, and B. F. Branstetter, "Basic principles and applications of 18F-FDG-PET/CT in oral and maxillofacial imaging: A pictorial essay," *Imaging Sci. Dent.*, vol. 44, no. 4, pp. 325–332, 2014.

[25] Center for Devices and Radiological Health, "Medical Imaging - Ultrasound Imaging." [Online].

Available: https://www.fda.gov/Radiation-EmittingProducts/RadiationEmittingProductsandProcedures/MedicalImaging/ucm115357.htm. [Accessed: 05-Dec-2017].

[26] "Conventional and spiral/helical CT." [Online]. Available: https://slideplayer.com/slide/10407630/#. [Accessed: 05-Aug-2018].

[27] T. Ishikawa *et al.*, "Cone-beam computed tomography correlates with conventional helical computed tomography in evaluation of lipiodol accumulation in HCC after chemoembolization," *PLoS One*, vol. 11, no. 1, pp. 6–11, 2016.

[28] M. Kumar, M. Shanavas, A. Sidappa, and M. Kiran, "Cone beam computed tomography - know its secrets.," *J. Int. oral Heal. JIOH*, vol. 7, no. 2, pp. 64–8, 2015.

[29] "Three-Dimensional Basics: CT vs. CBCT." [Online]. Available: https://carestreamdentalblogdotcom1.wordpress.com/2014/01/03/three-dimensional-basics-ct-vs-cbct/. [Accessed: 14-Dec-2017].

[30] M. Poon, C. Holborn, K. F. Cheng, W. W. K. Fung, and G. Chiu, "Evaluation of deformed image-based dose calculations for adaptive radiotherapy of nasopharyngeal carcinoma," *Med. Dosim.*, pp. 1–9, 2017.

[31] L. N. McDermott *et al.*, "3D in vivo dose verification of entire hypo-fractionated IMRT treatments using an EPID and cone-beam CT," *Radiother. Oncol.*, vol. 86, no. 1, pp. 35–42, 2008.

[32] O. Morin *et al.*, "Dose calculation using megavoltage cone-beam CT," *Int. J. Radiat. Oncol. Biol. Phys.*, vol. 67, no. 4, pp. 1201–1210, 2007.

[33] "LINAC Varian." [Online]. Available: https://images.dotmed.com/images/listingpics/1667777.jpg. [Accessed: 14-Dec-2017].

[34] P. Hauri, R. A. Hälg, and U. Schneider, "Technical note: No increase in effective dose from half compared to full rotation pelvis cone beam CT," *J. Appl. Clin. Med. Phys.*, vol. 18, no. 5, pp. 364–368, 2017.

[35] N. Colombo *et al.*, "ESMO-ESGO-ESTRO Consensus Conference on Endometrial Cancer: diagnosis, treatment and follow-up," *Ann. Oncol.*, vol. 27, no. 1, pp. 16–41, 2016.

[36] P. Petignat and M. Roy, "Diagnosis and management of cervical cancer," *Br. Med. J.*, vol. 335, no. 7623, pp. 765–768, 2007.

[37] "Velocity | Varian Medical Systems." [Online]. Available: https://www.varian.com/oncology/products/software/velocity?cat=overview. [Accessed: 19-Oct-2017].

[38] S. Oh and S. Kim, "Deformable Image Registration in Radiation Therapy," *Radiat. Oncol. J.*, vol. 35, no. 2, pp. 101–111, 2017.

[39] K. Jingu, "Radiology & radiation therapy use of deformable image registration for radiotherapy applications," *J. Radiol. Radiat. Ther.*, vol. 2, pp. 1–7, 2014.

[40] Y. Takayama *et al.*, "Evaluation of the performance of deformable image registration between planning CT and CBCT images for the pelvic region: Comparison between hybrid and intensity-based DIR," *J. Radiat. Res.*, vol. 58, no. 4, pp. 567–571, 2017.

[41] "Splines." [Online]. Available: https://en.wikipedia.org/wiki/Spline_(mathematics). [Accessed: 07-Nov-2017].

[42] "B-spline." [Online]. Available: https://en.wikipedia.org/wiki/B-spline. [Accessed: 07-Nov-2017].

[43] R. Shekhar, P. Lei, C. R. Castro-Pareja, W. L. Plishker, and W. D. D'Souza, "Automatic segmentation of phase-correlated CT scans through nonrigid image registration using geometrically regularized free-form deformation.," *Med. Phys.*, vol. 34, no. 7, pp. 3054–3066, 2007.

[44] M. Kessler and J. Pouliot, "Deformable image registration, contour propagation and dose mapping: 101 and 201," *Med. Phys.*, 2013.

[45] M. Fusella, F. R. Giglioli, C. Fiandra, and R. Ragona, "Evaluation of dose recalculation vs dose deformation in a commercial platform for deformable image registration with a computational phantom," *Med. Dosim.*, pp. 1–9, 2017.

[46] K. Jingu, "Radiology & radiation therapy: Use of deformable image registration for radiotherapy

applications," *J. Radiol. Radiat. Ther.*, vol. 2, pp. 1–7, 2014.
[47] K. S. C. Chao *et al.*, "Reduce in variation and improve efficiency of target volume delineation by a computer-assisted system using a deformable image registration approach.," *Int. J. Radiat. Oncol. Biol. Phys.*, vol. 68, no. 5, pp. 1512–21, Aug. 2007.
[48] C. A. Hvid, U. V. Elstrøm, K. Jensen, M. Alber, and C. Grau, "Accuracy of software-assisted contour propagation from planning CT to cone beam CT in head and neck radiotherapy," *Acta Oncol. (Madr).*, vol. 55, no. 11, pp. 1324–1330, 2016.
[49] X. Li *et al.*, "Comprehensive evaluation of ten deformable image registration algorithms for contour propagation between CT and cone-beam CT images in adaptive head & neck radiotherapy," *PLoS One*, vol. 12, no. 4, pp. 1–17, 2017.
[50] M. Thor, J. B. B. Petersen, L. Bentzen, M. Høyer, and L. P. Muren, "Deformable image registration for contour propagation from CT to cone-beam CT scans in radiotherapy of prostate cancer," *Acta Oncol. (Madr).*, vol. 50, no. 6, pp. 918–925, 2011.
[51] A. Kumarasiri *et al.*, "Changes in pharyngeal constrictor volumes during head and neck radiation therapy: Implications for dose delivery," *J. Cancer Res. Ther.*, vol. 12, no. 2, pp. 218–223, 2017.
[52] D. Yan, D. A. Jaffray, and J. W. Wong, "A model to accumulate fractionated dose in a deforming organ," *Int. J. Radiat. Oncol. Biol. Phys.*, vol. 44, no. 3, pp. 665–675, 1999.
[53] C. Zachiu, "Non-rigid CT/CBCT to CBCT registration for online external beam radiotherapy guidance," 2017.
[54] B. Schaly, J. A. Kempe, G. S. Bauman, J. J. Battista, and J. Van Dyk, "Tracking the dose distribution in radiation therapy by accounting for variable anatomy," *Phys. Med. Biol.*, vol. 49, no. 5, pp. 791–805, 2004.
[55] M. Moteabbed, G. C. Sharp, Y. Wang, A. Trofimov, J. A. Efstathiou, and H.-M. Lu, "Validation of a deformable image registration technique for cone beam CT-based dose verification," *Med. Phys.*, vol. 42, no. 1, pp. 196–205, 2014.
[56] C. Veiga *et al.*, "Toward adaptive radiotherapy for head and neck patients: Feasibility study on using CT-to-CBCT deformable registration for 'dose of the day' calculations," *Med. Phys.*, vol. 41, no. 3, p. 031703, 2014.
[57] C. Veiga *et al.*, "Toward adaptive radiotherapy for head and neck patients: Uncertainties in dose warping due to the choice of deformable registration algorithm.," *Med. Phys.*, vol. 42, no. 2, pp. 760–9, 2015.
[58] J. Vickress, J. Battista, R. Barnett, and S. Yartsev, "Representing the dosimetric impact of deformable image registration errors," *Phys. Med. Biol.*, vol. 62, no. 17, pp. N391–N403, 2017.
[59] L. C. Orlandini, M. Coppola, C. Fulcheri, L. Cernusco, P. Wang, and L. Cionini, "Dose tracking assessment for image-guided radiotherapy of the prostate bed and the impact on clinical workflow," *Radiat. Oncol.*, vol. 12, no. 1, p. 78, 2017.
[60] M. Cengiz *et al.*, "Comparison of intracavitary brachytherapy and stereotactic body radiotherapy dose distribution for cervical cancer.," *Brachytherapy*, vol. 11, no. 2, pp. 125–9, Mar. 2012.
[61] "Varian Launches New Smaller Calypso Beacon Transponder To Guide Radiation Therapy In Soft Tissue Tumors | Varian Medical Systems." [Online]. Available: https://www.varian.com/news/varian-launches-new-smaller-calypso-beacon-transponder-guide-radiation-therapy-soft-tissue. [Accessed: 24-Sep-2018].
[62] G. J. Kubicek *et al.*, "Stereotactic body radiotherapy as an alternative to brachytherapy in gynecologic cancer," *Biomed Res. Int.*, vol. 2013, 2013.
[63] M. Sen, Neilayan Sen, J. Zhou, R. Jozwiak, Y. Liao, and K. Kiel, "SBRT Boost as a Substitute for Brachytherapy in the Definitive Treatment of Gynecologic Malignancies With Radiotherapy," *Oncol. (willist. Park.)*, vol. 29, 2015.
[64] P. Latham and Y. Roudi, "Mutual information," *Scholarpedia*, 2009. [Online]. Available: http://www.scholarpedia.org/article/Mutual_information. [Accessed: 14-Nov-2017].
[65] *Velocity User Manual*. 2016.
[66] R. J. H. M. Steenbakkers *et al.*, "Reduction of observer variation using matched CT-PET for lung cancer delineation: A three-dimensional analysis," *Int. J. Radiat. Oncol. Biol. Phys.*, vol. 64, no. 2, pp. 435–448, 2006.
[67] D. D. Pestana and S. F. Velosa, *Introdução à probabilidade e à estatística*, 4th ed. Fundação

Calouste Gulbenkian, 2010.
[68] B. G. Tabachnick and L. S. Fidell, *Using multivariate statistics*, 5th ed. Pearson Education, Inc., 2007.
[69] J. F. Hair Jr., R. E. Anderson, R. L. Tatham, and W. C. Black, *Multivariate data analysis*. Pearson Education, Inc., 1998.
[70] E. J. Wuthrick *et al.*, "Institutional Clinical Trial Accrual Volume and Survival of Patients With Head and Neck Cancer," *J. Clin. Oncol.*, vol. 33, no. 2, pp. 156–164, 2015.
[71] R. D. Timmerman, "An Overview of Hypofractionation and Introduction to This Issue of Seminars in Radiation Oncology," *Semin. Radiat. Oncol.*, vol. 18, no. 4, pp. 215–222, 2008.